MCB
Journals.ASM.org

Leucine-Rich Repeat Kinase 1 Regulates Autophagy through Turning On TBC1D2-Dependent Rab7 Inactivation

Toshihiko Toyofuku,[a] Keiko Morimoto,[b] Shigemi Sasawatari,[a] Atsushi Kumanogoh[b]

Department of Immunology and Regenerative Medicine, Osaka University Graduate School of Medicine, Suita, Osaka, Japan[a]; Department of Respiratory Medicine, Allergy and Rheumatic Diseases, Osaka University Graduate School of Medicine, Suita, Osaka, Japan[b]

Autophagy is a conserved process that enables catabolic and degradative pathways. Rab family proteins, which are active in the GTP-bound form, regulate the transport and fusion of autophagosomes. However, it remains unclear how each cycle of Rab activation and inactivation is precisely regulated. Here, we show that leucine-rich repeat kinase 1 (LRRK1) regulates autophagic flux by controlling Rab7 activity in autolysosome formation. Upon induction of autophagy, LRRK1 was recruited via an association with VAMP7 to the autolysosome, where it activated the Rab7 GTPase-activating protein (GAP) TBC1D2, thereby switching off Rab7 signaling. Consistent with this model, LRRK1 deletion caused mice to be vulnerable to starvation and disrupted autolysosome formation, as evidenced by the accumulation of enlarged autolysosomes with undegraded LC3-II and persistently high levels of Rab7-GTP. This defect in autophagic flux was partially rescued by a mutant form of TBC1D2 with elevated Rab7-GAP activity. Thus, the spatiotemporal regulation of Rab7 activity during tunicamycin-induced autophagy is regulated by LRRK1.

Autophagy is a conserved catabolic process in eukaryotic cells that is critical for a wide range of physiological processes, such as embryonic development and establishment of self-tolerance in the immune system (1). Autophagy is impaired in many human diseases, including Parkinson's disease, Crohn's disease, and cancers (2). A complex network of core components (autophagy-related or Atg proteins) regulates the initiation and maturation of autophagosomes by recruiting proteins required for membrane elongation, movement, and fusion with a number of vesicular compartments. One of the core proteins, Atg8/LC3 (microtubule-associated light chain 3), is converted to the lipidated form (LC3-II) when autophagy is induced; this modification is essential for expansion and fusion of membranes to form autophagosomes, which are characterized by a double-membrane vesicular structure (3, 4). Ultimately, autophagosome contents are degraded upon fusion with lysosomes (autolysosomes) (4, 5).

Although membrane fusion is required at multiple steps within autophagic flux, the underlying mechanisms are not well understood. Upon initiation of autophagy, the isolation membrane grows and seals itself to form an autophagosome; this process is independent of the SNARE proteins involved in conventional membrane fusion (3). Once the autophagosome has formed, fusion with the vacuole proceeds essentially identically to endocytic fusion in a reaction involving SNARE proteins, Rab GTPase, and the homotypic vacuole fusion and protein sorting (HOPS) complex (6). SNARE proteins such as TI-VAMP/VAMP7, Rab7, and the HOPS complex have been implicated in late endosome-lysosome fusion (7, 8).

The Roco family of proteins is characterized by two conserved domains: a Ras-like GTPase domain (Roc) and a C-terminal domain (COR) (9). Vertebrate genomes contain four ROCO genes: *LRRK1*, *LRRK2*, *DAPK1* (death-associated kinase 1), and *MFHAS1* (malignant fibrous histiocytoma amplified sequence 1). Mutations in *LRRK2* are associated with both familial and sporadic Parkinson's disease, a progressive neurodegenerative disorder with limited therapeutic options. Via interactions with multiple molecules, leucine-rich repeat kinase 2 (LRRK2) functions in apoptosis (10), protein synthesis (11, 12), and cytoskeletal dynamics (13–15). Recently, several reports have demonstrated that LRRK2 controls autophagy (16–20). Owing to this diversity of function, despite intense interest and extensive study, the mechanisms by which *LRRK2* mutations cause neurodegeneration remain unclear. Given the high degree of sequence similarity between LRRK1 and LRRK2, it is plausible that LRRK1 has analogous functional properties. However, Parkinson's disease-related mutations in LRRK1 have not been identified (21). The expression of LRRK1 and LRRK2 differs among organs; LRRK2 is highly expressed in the brain, kidneys, and immune cells, whereas LRRK1 is nearly absent from these organs. Moreover, *Lrrk2*$^{-/-}$ mice exhibit accumulation and aggregation of α-synuclein and apoptotic cells in the kidney (20). In order to shed more light on the roles of the LRRK proteins, deficiency of each LRRK-encoding gene should be studied individually in murine models.

To investigate LRRK1 function *in vivo*, we generated LRRK1-deficient mice. These mice exhibited vulnerability to starvation, indicative of impaired of autophagy. Upon induction of autophagy, *Lrrk1* deletion induced accumulation of enlarged autolysosomes with (i) increased LC3-II due to a defect in lysosomal degradation during autophagy and (i) reduced conversion of Rab7-GTP to GDP due to a reduction in the Rab7 GTPase-activating protein (GAP) activity of TBC1D2. These results suggested that LRRK1 promotes Rab7 inactivation during autophagy. In

Received 22 January 2015 **Returned for modification** 11 February 2015
Accepted 19 June 2015

Accepted manuscript posted online 22 June 2015

Citation Toyofuku T, Morimoto K, Sasawatari S, Kumanogoh A. 2015. Leucine-rich repeat kinase 1 regulates autophagy through turning on TBC1D2-dependent Rab7 inactivation. Mol Cell Biol 35:3044–3058. doi:10.1128/MCB.00085-15.

Address correspondence to Toshihiko Toyofuku, toyofuku@imed3.med.osaka-u.ac.jp.

Supplemental material for this article may be found at http://dx.doi.org/10.1128/MCB.00085-15.

doi:10.1128/MCB.00085-15

contrast to the functional role of LRRK1 in autophagic flux, LRRK2 deletion or Parkinson's disease-related mutation disrupts the conversion of LC3-I to LC3-II (16, 18, 19); moreover, pathogenic LRRK2 decreases Rab7 activity, thereby delaying epidermal growth factor receptor degradation (22) and intraneuronal protein sorting (23). Thus, LRRK2 probably promotes Rab7 activation during autophagy. Taken together, these observations suggest that LRRK1 and LRRK2 cooperatively promote the Rab7 activation-and-inactivation cycle during autophagy.

MATERIALS AND METHODS

Generation of *Lrrk1*$^{-/-}$ mice. Generation of *Lrrk1* knockout mice was performed in collaboration with UNITECH (Chiba, Japan). A FRT-neomycin-FRT-LoxP validated cassette was inserted downstream of exon 5, and a LoxP site was inserted upstream of exon 4 (see Fig. S1A to C in the supplemental material). Following homologous recombination in embryonic stem (ES) cells, ES cell injection into blastocytes, and generation of chimeras, the Neo cassette was deleted by breeding chimeras with C57BL/6J mice expressing Flp recombinase. Heterozygous floxed mice were bred with C57BL/6J mice expressing Cre recombinase under the control of the CAG promoter. Offspring were subsequently bred with each other to generate Cre^{+} *Lrrk1*$^{flox/flox}$ (*Lrrk1*$^{-/-}$) and Cre^{-} *Lrrk1*$^{flox/flox}$ controls (*Lrrk1*$^{+/+}$). We used constitutive *Lrrk1*$^{-/-}$ animals where the knockout allele had been backcrossed in C57BL/6J mice for five generations. All experiments were approved by our institution's animal care and use committee.

Isolation of MEFs from mouse embryos. *Lrrk1*$^{+/+}$ and mutant mouse embryo fibroblasts (MEFs) were prepared and cultured as described previously (24). Autophagy was induced by treatment with tunicamycin (1 μg/ml) for 2 h in full-nutrient Dulbecco's modified Eagle's medium (DMEM). Alternatively, cells were starved for 2 h in glucose-free DMEM containing 2-deoxy-D-glucose (20 μM).

Generation of expression vectors and site-directed mutagenesis. cDNAs encoding mouse ARHGAP22, LRRK1, Rab7, TBC1D2, and VAMP7 were synthesized by PCR and ligated into pc3XFLAG-CMV-14 (Sigma-Aldrich), pcDNA3.1/V5-His (Invitrogen Life Technologies), pCMV-HA (Clontech Laboratories), or pCMV-Myc (Clontech Laboratories). LRRK1 deletion constructs LRRK1-D1 (amino acids [aa] 1 to 630), LRRK1-D2 (aa 1 to 1230), LRRK1-D3 (aa 601 to 2019), and LRRK1-D4 (aa 1224 to 2019) were synthesized by PCR and ligated into FLAG-CMV-3 or -4 (Sigma-Aldrich). TBC1D2 deletion constructs ΔPH-TBC (aa 1 to 165) and ΔTBC-TBC (aa 166 to 922) were synthesized by PCR and ligated into pCMV-HA and pCMV-Myc. Previous studies showed that mutations within the activation segment of the kinase domain of Lrrk2 resulted in a loss (mutation of D^{1994} to A) of Lrrk2 kinase activity (25, 26). A sequence comparison revealed that residue D^{1386} in Lrrk1 corresponds to D^{1994} in Lrrk2 (see Fig. S1D in the supplemental material), and thus, mutation of D^{1386} to A was performed to create kinase-dead LRRK1(D1386A) (see Fig. S1E). Mutation of T^{22} to N or Q^{67} to L in Rab7 (Rab7T22N or Rab7Q67L) was performed to create constitutively active Rab7 and dominant negative Rab7, respectively (see Fig. S1F) (27). Each mutation was created with the QuikChange site-directed mutagenesis kit (Stratagene, La Jolla, CA). To visualize transfected MEFs in live-imaging experiments, the constructs were ligated into pEGFP-N1 or pDsRed-monomer (Clontech Laboratories).

RNAi. The pcDNA6.2-GW-miR plasmid (Clontech Laboratories) was modified by deleting the gene for green fluorescent protein (GFP) by using the flanking DraI sites. To increase RNA interference (RNAi) efficiency, short hairpin RNA (shRNA) oligonucleotides specific for two target sequences of mouse AHRGAP22, TBC1D2, and VAMP7 (see Table S1 in the supplemental material) were designed and ligated into the modified pcDNA6.2-GW-miR expression vector. Cultured cells were transfected with shRNA vectors by Nucleofector technology (Amaxa Biosystems, Cologne, Germany). Transfected cells were identified by their red color under fluorescence microscopy. The efficiency of knockdown was verified by Western blot assay.

Antibodies, immunoprecipitation, and immunoblotting. The antibodies used in this study included anti-ARHGAP22 (Abcam), anti-LC3 (MBL), anti-LRRK1 (Abgent), anti-p62 (Abcam), anti-Rab7 (Abcam), anti-TBC1D2 (Abcam), anti-VAMP7 (Abcam), anti-FLAG (Sigma-Aldrich), antihemagglutinin (anti-HA; Sigma-Aldrich), and anti-Myc (MBL) antibodies. Transfected cells were incubated for 2 days, harvested, and then lysed in lysis buffer (50 mM Tris-HCl at pH 8.0, 150 mM NaCl, 0.1% SDS) for immunoblotting or in TNE buffer (50 mM Tris-HCl, 150 mM NaCl, 5 mM EDTA, 1% NP-40, 0.25% Na-deoxycholate, 1 mM NaF) for immunoprecipitation and immunoblotting. Immunoprecipitation and immunoblot analyses were performed by using standard protocols.

Rab7 activation assay. Rab7-GTP levels were determined with a Rab7 activation assay kit (Abcam). Briefly, cells were incubated with tunicamycin (1 μg/ml) or with glucose-free DMEM containing 2-deoxy-D-glucose (20 μM) for 2 h, and lysates were immunoprecipitated with the anti-Rab7-GTP monoclonal antibodies bound to protein A/G-agarose. The precipitated Rab7-GTP was detected by immunoblotting with a rabbit anti-Rab7 polyclonal antibody. The level of Rab7-GTP was expressed as a percentage of the total level of endogenous Rab7. Control values were arbitrarily assigned a value of 1.

Rac1 activation assay. Rac1-GTP levels were determined with the Rac1 activation assay kit (Upstate). Briefly, cells were incubated with tunicamycin (1 μg/ml) or with glucose-free DMEM containing 2-deoxy-D-glucose (20 μM) for 2 h, and lysates were incubated with the PAK-1 protein binding domain (PBD) bound to glutathione-agarose to pull down Rac1-GTP, which was detected by immunoblotting with an anti-Rac1 monoclonal antibody. The level of Rac1-GTP was expressed as a percentage of the total level of endogenous Rac1. Control values were arbitrarily assigned a value of 1.

Cathepsin assay. Cathepsins D and E cleave the fluorogenic cathepsin D/E substrate (Enzo), resulting in enhanced fluorescence. Cells (1×10^6/well) were collected and lysed in buffer (50 mM sodium acetate [pH 4.0], 0.1% Triton X-100). After centrifugation (7,000 rpm for 10 min), supernatants were supplemented with fluorogenic cathepsin D/E substrate (final concentration, 20 μM) and incubated at 40°C for 10 min; the reactions were stopped by the addition of 5% trichloroacetic acid. Enzyme activity was determined by measuring fluorescence (excitation wavelengths, 320 to 340 nm; emission wavelengths, 393 to 420 nm).

Hexosaminidase assay. Hexosaminidase hydrolyzes 4-nitrophenyl-*N*-acetyl-β-D-glucosaminide (Sigma), thereby producing 4-nitrophenol, which can be detected spectrophotometrically at 405 nm to determine enzyme activity. Cells (1×10^5/well) were collected and lysed in buffer (0.1 M citrate [pH 4.5], 0.1% Triton X-100). After centrifugation (7,000 rpm for 10 min), supernatants were supplemented with *p*-nitrophenyl-*N*-acetyl-β-D-glucosaminide (final concentration, 1 mM) and incubated at 37°C for 1 h; the reactions were stopped by the addition of 200 mM borate buffer (pH 9.8). Enzyme activity was determined by measuring absorbance at 405 nm.

Fluid-phase endocytosis assay by fluorescent dextran uptake. Fluorescent dextran is taken up by vesicles that are part of the endocytic pathway, which is composed of endosomes and lysosomes. The morphological change in endosomes was examined with fluorescein isothiocyanate (FITC)-dextran (Molecular Probes). Cells plated on glass bottom dishes were incubated with FITC-dextran (5 mg/ml) for 2.5 h. Endosomes were visualized with a laser scanning confocal microscope (LSM 5 EXCITER [ver. 4.2]; Zeiss, Thornwood, NY). The acidification of lysosomes was examined with LysoSensor yellow/blue dextran (Molecular Probes), which exhibits a pH-dependent increase in fluorescence intensity upon acidification. Cells plated on the glass bottom dish were incubated with LysoSensor yellow/blue dextran (5 mg/ml) for 2.5 h. LysoSensor is a UV-excited fluorophore with emission maxima at 450 and 530 nm that are proportional to the pH. A higher 530/450-nm ratio correlates with a lower pH (see Fig. S5 in the supplemental material). The labeled cells were

observed with a laser scanning confocal microscope with excitation at 360 nm, a 450-nm emission filter, and a 515-nm long-pass emission filter.

LipidTOX neutral lipid staining. The intracellular accumulation of neutral lipids was stained with HCS LipidTOX red (Molecular Probes). Cells plated on the glass bottom dish were starved for 4 h and incubated with HCS LipidTOX red for last 30 min. Lipid droplets were visualized by fluorescence microscopy.

Yeast two-hybrid library screening. *Saccharomyces cerevisiae* strain AH109 was transformed with bait plasmid pGBDU-C1 encoding the N terminus (aa 1 to 615) or the C terminus (aa 1224 to 2019) of LRRK1 and screened against a mouse brain cDNA Matchmaker library (BD Biosciences). Interacting proteins were identified by plasmid sequencing and BLAST searching. In order to confirm the interaction with the identified prey DNA, the indicated region of LRRK1 and the prey DNA were cloned into the GAL4 DNA binding domain and GAL4 DNA activation domain plasmids, respectively. The resultant plasmids were transformed into yeast strain PJ69-4A, and the interaction between the two proteins was tested in the yeast two-hybrid system. Interactions of binding and activation domain fusion proteins were scored on the basis of yeast growth.

Protein-protein interaction analysis by fluorescence microscopy. The CoralHue Fluo-chase kit was purchased from Amalgaam (Medical & Biological Laboratories). This reporter system is based on fusion proteins of fragments of monomeric coral fluorescent reporter protein (monomeric Kusabira-Green [mKG]). In this system, one protein of interest is fused to the N-terminal fragment of divided mKG and the other protein of interest is fused to the C-terminal fragment of divided mKG. In cells transfected with the two constructs, close positioning or association of the two proteins results in detectable green fluorescence. VAMP7 (aa 1 to 180) was fused with the N-terminal fragment of mKG (mKG-N), and LRRK1-D1 (aa 1 to 630) was fused with the C-terminal fragment of mKG (mKG-C). MEFs were transfected with a pair of mKG constructs by electroporation. Twenty-four hours after transfection, transfected cells were observed with a laser scanning confocal microscope with excitation at 494 nm and a 506-nm emission filter.

Live-cell imaging. Cells transfected with chromophore-fused constructs were treated with tunicamycin (1 μg/ml) or glucose-free DMEM containing D-glucose (20 μM) for 2 h, and lysosomes were visualized with LysoTracker (Molecular Probes). Cells were imaged with an LSM 5 EXCITER (ver. 4.2) inverted confocal microscope (Carl Zeiss MicroImaging). For colocalization analysis, Pearson's coefficients were calculated with the Imaris software. All colocalization calculations were performed on more than 50 cells from at least three independent experiments.

Electron microscopy. Livers were removed and incubated overnight in 0.1 M phosphate buffer containing 3.5% glutaraldehyde. The tissue was then incubated in 2% osmium tetroxide, stained with 2% uranyl acetate, and embedded in Spurr's resin. Ultrathin sections were collected in Formvar-coated slot grids and stained with lead citrate. Micrographs were obtained at ×5,000 or ×12,000 magnification.

RESULTS

The phenotype of LRRK1-deficient mice. To examine the LRRK1-deficient phenotype, we bred $Lrrk1^{flox/flox}$ mice with a line of transgenic mice that express the Cre recombinase under the control of the CAG promoter in oocytes (see Fig. S1 in the supplemental material). $Lrrk1^{-/-}$ mice, obtained by breeding $Lrrk1^{+/-}$ mice, were born at Mendelian frequency. Although homozygous mice appeared normal at birth and had no apparent developmental defects by histological analysis, half of the $Lrrk1^{-/-}$ mice died within 1 day after birth in multiple cohorts for several years (Fig. 1A). We speculated that $Lrrk1^{-/-}$ mice could survive *in utero* by virtue of nutrients supplied through the placenta but could not survive when that supply terminated after birth. Most $Lrrk1^{-/-}$ neonates were found with milk in their stomachs, excluding the possibility that they had a suckling defect. We tested the survival time of $Lrrk1^{-/-}$ neonates under starvation conditions. $Lrrk1^{+/+}$ and heterozygous mice died at 28.7 ± 3.7 h, whereas $Lrrk1^{-/-}$ mice died at 19.6 ± 2.1 h ($P < 0.01$) (Fig. 1B). Electron micrographs of livers from $Lrrk1^{+/+}$ mice revealed the presence of autophagosomes following 1 day of starvation (Fig. 1C, arrowhead), whereas livers from $Lrrk1^{-/-}$ mice contained large amounts of glycogen granules following feeding (Fig. 1C, asterisk) and their lysosomes were swollen with amorphous membranous materials (Fig. 1C, arrows). These results suggested that *Lrrk1* deletion caused lysosomal dysfunction.

In mammals, a critical source of energy immediately after birth is provided by autophagy, which is necessary for the turnover of cellular components, particularly in response to starvation (28, 29). Upon starvation, LC3 is upregulated, recruited to the autophagosome, and degraded in the lysosome (30), while p62, a ubiquitin-binding protein, binds to LC3 and is degraded in the lysosome (31). Thus, levels of LC3-II and p62 can be used as markers to study autophagic flux. We examined the induction of autophagy by detecting the conversion of endogenous LC3-I to LC3-II and p62 levels (Fig. 1D and E). The amounts of LC3-II and p62 in liver homogenates from $Lrrk1^{+/+}$ mice transiently increased on the day of birth, suggesting that massive autophagy was induced in these mice under physiological conditions, probably in response to nutrient limitation. In contrast, in the liver homogenate of $Lrrk1^{-/-}$ mice, the levels of LC3-II and p62 increased after birth and remained high for up to 9 h. These findings suggested that $Lrrk1^{-/-}$ mice have defects in autophagic flux, which may make them vulnerable to starvation.

Next, we analyzed autophagosome formation in MEFs prepared from $Lrrk1^{+/+}$ and $Lrrk1^{-/-}$ mouse embryos. We treated these MEFs with starvation (glucose-free medium containing D-glucose [20 μM]) or tunicamycin (1 μg/ml), an inhibitor of acylglucosamine phosphotransferase that induces the endoplasmic reticulum (ER) stress response and autophagy (Fig. 1F and G) (32, 33). Under the control condition, $Lrrk1^{-/-}$ MEFs contained higher levels of LC3-II and p62 than did $Lrrk1^{+/+}$ MEFs, suggesting that autophagosome formation was elevated in the $Lrrk1^{-/-}$ MEFs. In response to tunicamycin treatment, $Lrrk1^{+/+}$ MEFs contained higher levels of LC3-II and p62, whereas $Lrrk1^{-/-}$ MEFs exhibited no further increase in their LC3-II and p62 levels. In response to starvation, the short incubation (15 to 30 min) with glucose-free medium containing D-glucose increased LC3-II, while the longer incubation (>1 h) used in this study decreased LC3-II in MEFs (data not shown). $Lrrk1^{-/-}$ MEFs contained higher levels of LC3-II and p62 than did $Lrrk1^{+/+}$ MEFs. These results suggested that *Lrrk1* deletion blocks autophagosome maturation, including autophagosome-lysosome fusion or lysosomal degradation. To determine whether loss of LRRK1 enhances autophagosome synthesis, we blocked LC3-II and p62 autophagosome degradation with bafilomycin A1, a lysosomal proton pump inhibitor (34). Upon treatment with bafilomycin A1, $Lrrk1^{-/-}$ MEFs exhibited no further increase in LC3-II levels relative to $Lrrk1^{+/+}$ cells. Thus, *Lrrk1* deletion may impair autophagosome maturation rather than increase autophagosome synthesis.

Autophagosome degradation is impaired in $Lrrk1^{-/-}$ cells. To test the possibility that autophagosome degradation is blocked in $Lrrk1^{-/-}$ MEFs, we used a tandem-tagged GFP-mCherry-LC3 probe, which can dissect whether an autophagosome has fused with a lysosome on the basis of the distinct chemical properties of the GFP and mCherry fluorophores (35). Under nonlysosomal

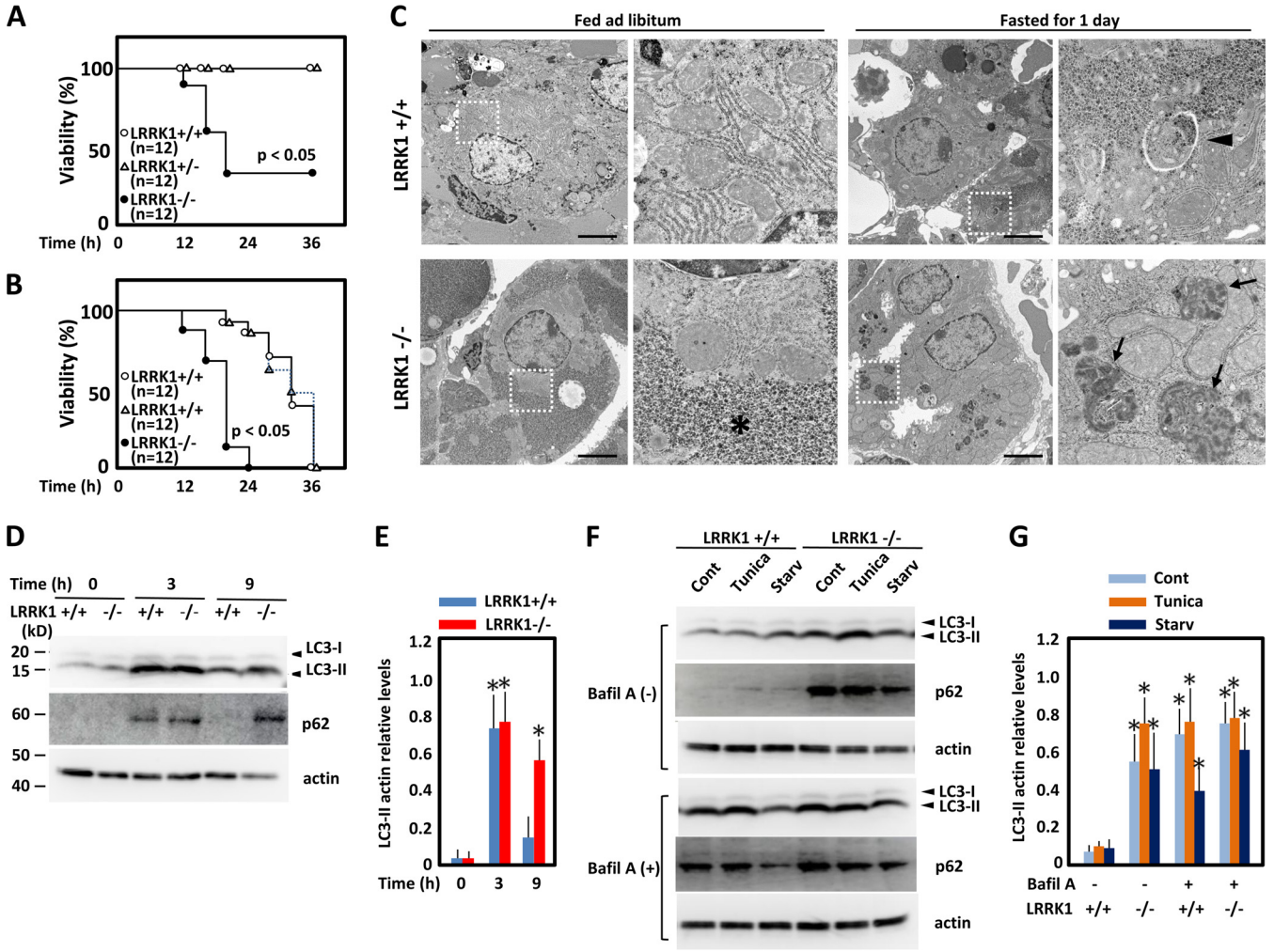

FIG 1 Autophagy is impaired in *Lrrk1*$^{-/-}$ mice. (A and B) Kaplan-Meier curves of survival of newborn mice. Neonates were monitored in a humidified chamber with (A) and without (B) feeding. (C) Electron micrographs of liver samples from *Lrrk1*$^{+/+}$ and *Lrrk1*$^{-/-}$ mice fed *ad libitum* or fasted for 1 day. Magnified images of the boxed areas are shown on the right. The arrowhead indicates an autophagosome, and arrows indicate enlarged lysosomes containing amorphous materials. The asterisk indicates glycogen granules. Scale bars, 1 μm. (D) Immunoblotting of LC3 and p62. Liver homogenates were prepared from neonates at 0, 3, and 6 h after birth. (E) Levels of LC3 and p62 were corrected for actin levels. Error bars represent standard deviations from three independent experiments. One-way analysis of variance with Tukey's *post hoc* test: *, $P < 0.05$ compared to control *Lrrk1*$^{+/+}$ mice at 0 h. (F) Immunoblotting of LC3 and p62. *Lrrk1*$^{+/+}$ and *Lrrk1*$^{-/-}$ MEFs were treated with the control (Cont) or tunicamycin (Tunica; 1 μg/ml) or starvation (Starv) in the presence or absence of bafilomycin (Bafil) A1 (400 nM), and endogenous LC3 and p62 levels were measured by blot analysis. (G) Values were normalized against actin levels. The error bars represent standard deviations from three independent experiments. One-way analysis of variance with Tukey's *post hoc* test: *, $P < 0.05$ compared to control *Lrrk1*$^{+/+}$ MEFs in the absence of bafilomycin.

and nearly neutral pH conditions, both GFP and mCherry retain their fluorescence. However, the low pH in the lumen of the lysosome quenches the signal from GFP but not that of mCherry. Upon starvation and tunicamycin treatment of cells expressing this probe, GFP- and mCherry-positive autophagosomes formed and surrounded the lysosome; loss of the GFP signal (while the mCherry signal was retained) took place within 60 min (Fig. 2A). In *Lrrk1*$^{-/-}$ MEFs, both treatments produced enlarged structures that retained the GFP signal, which was contained in the lysosome. The introduction of LRRK1 but not kinase-dead LRRK1(D1386A) into *Lrrk1*$^{-/-}$ MEFs rescued the morphological changes (Fig. 2B). These results suggested that *Lrrk1* deletion blocks autophagosome-lysosome fusion and that kinase activity of LRRK1 is required for this process. Next, we estimated the pH of lysosomes with LysoSensor blue/yellow dextran, which has pH-sensitive emission peaks (Fig. 2C) (36). In *Lrrk1*$^{+/+}$ MEFs treated with LysoSensor-dextran for 3 h, endosomes containing LysoSensor-dextran were at lower pH under physiological conditions, whereas in *Lrrk1*$^{-/-}$ MEFs treated with LysoSensor-dextran, endosomal pH was closer to neutral (Fig. 2C). *Lrrk1*$^{-/-}$ MEFs also exhibited enlarged vesicles containing FITC-dextran (Fig. 2D and E). These results indicated that autophagosome degradation is impaired in *Lrrk1*$^{-/-}$ MEFs, resulting in the enlargement of undegraded contents.

In addition to the autophagosome degradation, lysosomes are involved in lipid catabolism and proteolysis. To study the role of LRRK1 in lipid catabolism, we treated MEFs with a fluorescently labeled phospholipid (LipidTOX red). Upon starvation, *Lrrk1*$^{-/-}$ MEFs exhibited considerable accumulation of LipidTOX Red in endocytic vesicles (Fig. 2F and G), indicating that

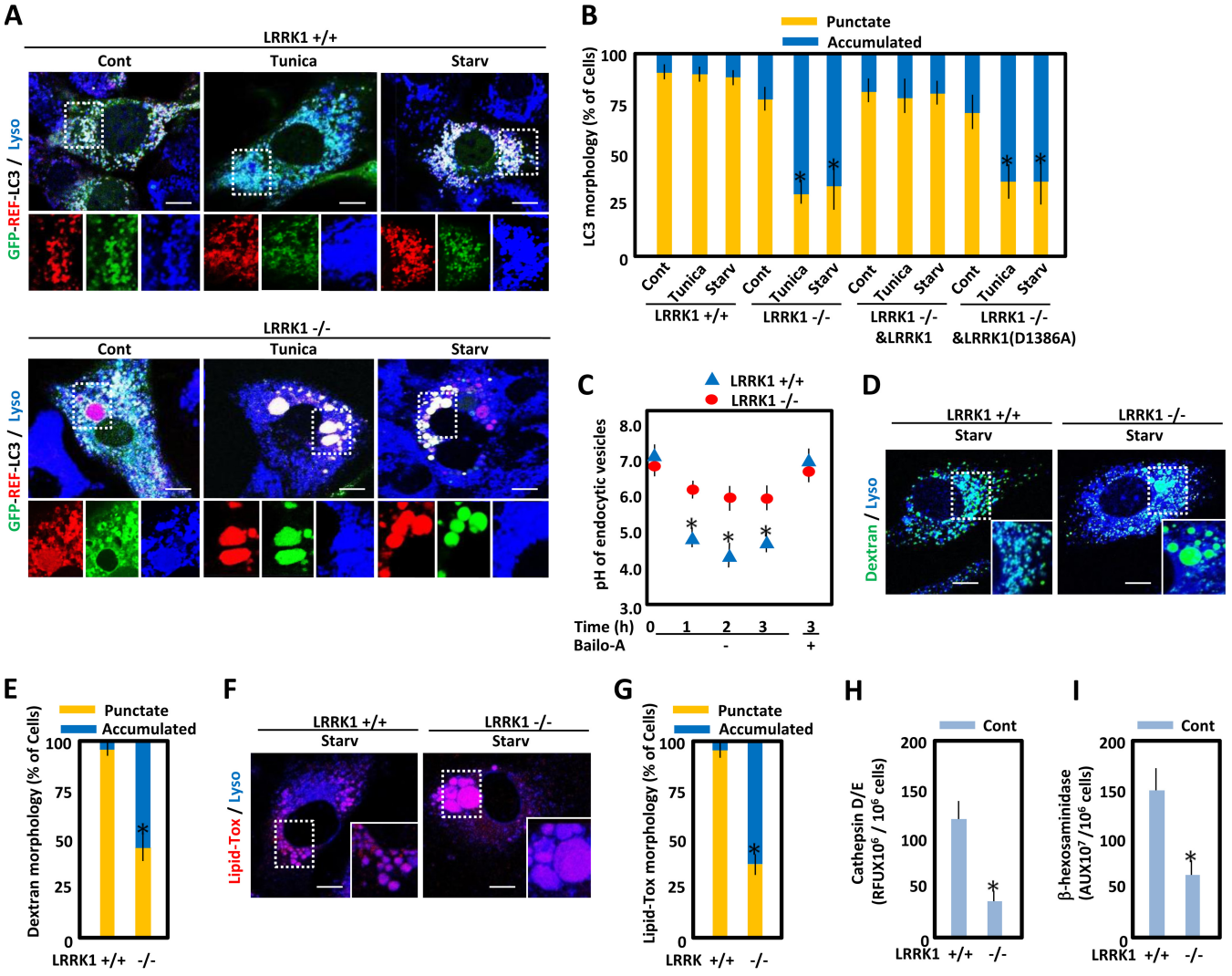

FIG 2 Autolysosome formation is impaired in *Lrrk1*$^{-/-}$ MEFs. (A) *Lrrk1*$^{+/+}$ and *Lrrk1*$^{-/-}$ MEFs expressing GFP/mCherry-LC3 were treated under control (Cont), tunicamycin (Tunica), or starvation (Starv) conditions for 4 h and stained with LysoTracker for the last 30 min. Merged images of MEFs (top) and magnified images of the boxed areas (bottom) are shown. Scale bars, 10 μm; arrowheads, fusion of LC3-positive vesicles with lysosomes was blocked in MEFs transfected with VAMP7 shRNA. (B) Percentages of cells harboring punctate or accumulated GFP/mCherry-LC3 in *Lrrk1*$^{+/+}$ and *Lrrk1*$^{-/-}$ MEFs expressing LRRK1 with or without mutations. LC3 morphology was classified as follows: punctate, many discrete GFP/mCherry-LC3 dots, crescent-shaped, or circular signals on or near lysosomes; accumulated, at least one large GFP/mCherry-LC3 clump (>2 μm) on or near lysosomes. The error bars represent standard deviations from three independent experiments. Over 50 cells were counted in each experiment. One-way analysis of variance with Tukey's *post hoc* test: *, $P < 0.005$ compared to control *Lrrk1*$^{+/+}$ MEFs. (C) *Lrrk1*$^{+/+}$ and *Lrrk1*$^{-/-}$ MEFs were incubated with LysoSensor yellow/blue dextran for 3 h. Dual emission was measured at 450 and 530 nm for LysoSensor yellow/blue-labeled cells. The 530/450-nm fluorescence ratio was calculated, and the pH was obtained from a pH calibration curve. (D) *Lrrk1*$^{+/+}$ and *Lrrk1*$^{-/-}$ MEFs were incubated with FITC-dextran for 2.5 h under starvation conditions and stained with LysoTracker for last 30 min. Merged images of MEFs and magnified images of the boxed areas (insets) are shown. Scale bars, 10 μm. (E) Percentages of cells harboring punctate or accumulated FITC-dextran are shown. Dextran morphology was classified as follows: punctate, many discrete dextran dots; accumulated, at least one large (>2-μm) dextran clump. The error bars represent standard deviations from three independent experiments. Over 50 cells were counted in each experiment. One-way analysis of variance with Tukey's *post hoc* test: *, $P < 0.05$ compared to *Lrrk1*$^{+/+}$ MEFs. (F) *Lrrk1*$^{+/+}$ and *Lrrk1*$^{-/-}$ MEFs under starvation conditions were stained with LipidTOX red and LysoTracker for 30 min. Merged images of MEFs and magnified images of the boxed areas (insets) are shown. Scale bars, 10 μm. (G) Percentages of cells harboring punctate or accumulated lipid droplets stained with LipidTOX. LipidTOX morphology was classified as follows: punctate, many discrete lipid dots; accumulated, at least one large (>2-μm) LipidTOX clump. The error bars represent standard deviations from three independent experiments. Over 50 cells were counted in each experiment. One-way analysis of variance with Tukey's *post hoc* test: *, $P < 0.005$ compared to *Lrrk1*$^{+/+}$ MEFs. (H) Cathepsin D/E activity in *Lrrk1*$^{+/+}$ and *Lrrk1*$^{-/-}$ MEFs under control conditions were evaluated. Values are expressed in relative fluorescence units (RFU) per 10^6 cells. One-way analysis of variance with Tukey's *post hoc* test: *, $P < 0.05$ compared to control *Lrrk1*$^{+/+}$ MEFs. (I) Hexosaminidase activity in *Lrrk1*$^{+/+}$ and *Lrrk1*$^{-/-}$ MEFs under control conditions were evaluated. Values are expressed in absorbance units (AU) per 10^6 cells. One-way analysis of variance with Tukey's *post hoc* test: *, $P < 0.05$ compared to control *Lrrk1*$^{+/+}$ MEFs.

these cells had defects in lipid catabolism. In addition, we measured the total enzymatic activity of lysosomal enzymes with fluorogenic substrates for cathepsin D/E and β-hexosaminidase. Enzyme activities were lower in *Lrrk1*$^{-/-}$ MEFs than in *Lrrk1*$^{+/+}$ MEFs (Fig. 2H and I). These results suggested that *Lrrk1*$^{-/-}$ MEFs contain defects in the sorting of lysosomal enzyme-containing endosomes to lysosomes from the Golgi apparatus or defects in enzyme-containing endosome-lysosome fusion.

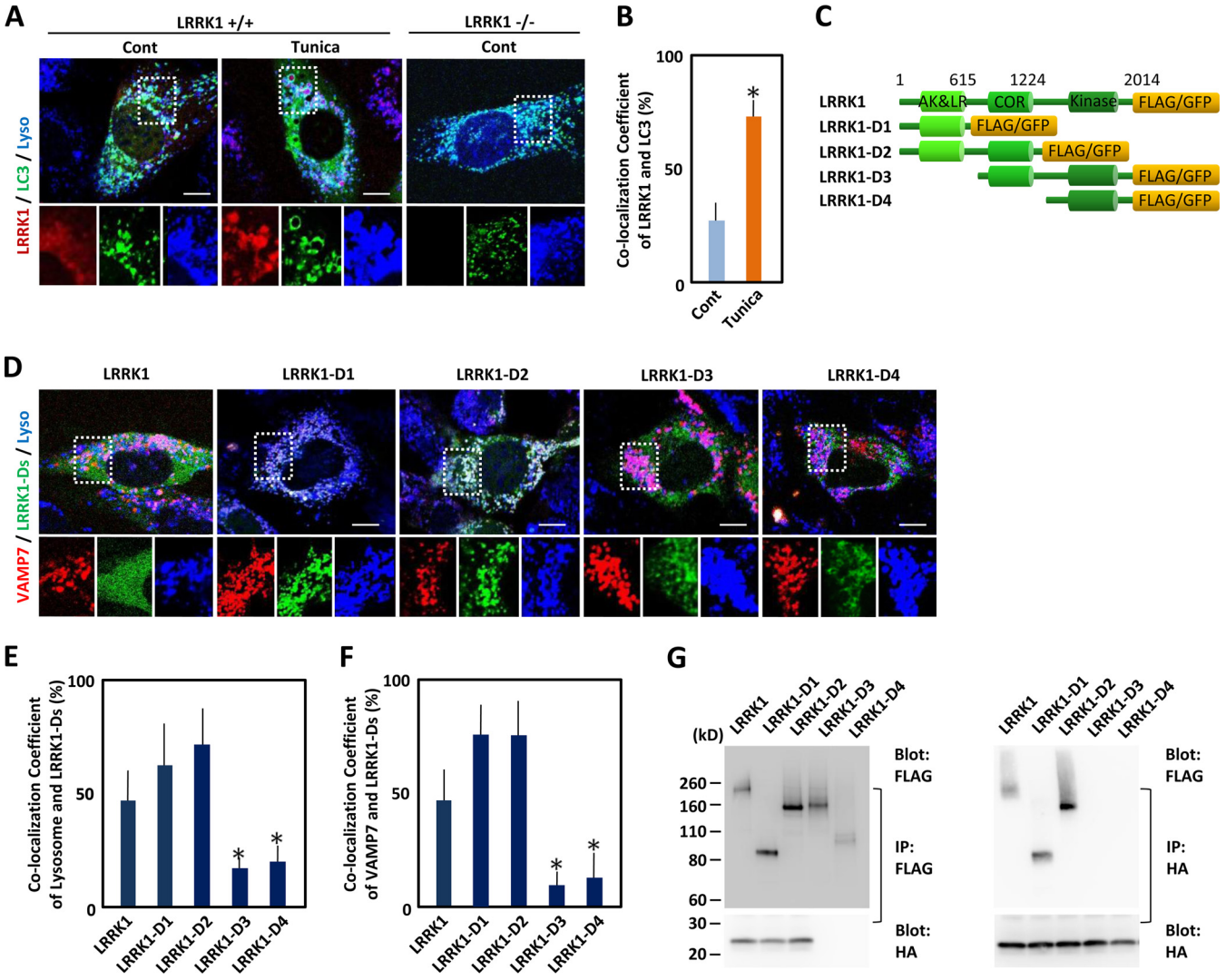

FIG 3 LRRK1 interacts with VAMP7. (A) LRRK1$^{+/+}$ MEFs expressing GFP-LC3 and LRRK1-Red were subjected to control (Cont) or tunicamycin (Tunica) treatment for 4 h and then stained with LysoTracker for the last 30 min. Merged images of MEFs (top) and magnified images of the boxed areas (bottom) are shown. Scale bars, 10 μm. (B) Immunofluorescence colocalization of GFP-LC3 and LRRK1-Red expressed in *Lrrk1*$^{+/+}$ MEFs. The colocalization of two proteins was analyzed by Pearson and Spearman correlation coefficients. The error bars represent standard deviations from three independent experiments. Over 50 cells were counted in each experiment. One-way analysis of variance with Tukey's *post hoc* test: *, $P < 0.005$ compared to control *Lrrk1*$^{+/+}$ MEFs. (C) Diagram showing full-length and truncated LRRK1 proteins. Amino acids are noted at the top. AK&LR, ankyrin-repeat and leucine-rich repeat; COR, C terminus of Ras of complex proteins (Roc) domain; kinase, Ser/Thr kinase domain. (D) *Lrrk1*$^{-/-}$ MEFs expressing different mutant forms of LRRK1-GFP and VAMP7-Red were stained with LysoTracker for 30 min. Merged images of MEFs (top) and magnified images of the boxed areas (bottom) are shown. Scale bars, 10 μm. (E, F) Immunofluorescence colocalization of different mutant forms of LRRK1-GFP and lysosomes in LRRK1$^{-/-}$ MEFs (E) and different mutant forms of LRRK1-GFP and VAMP7-Red in *Lrrk1*$^{-/-}$ MEFs (F). The colocalization of two proteins was analyzed by Pearson and Spearman correlation coefficients. The error bars represent standard deviations from three independent experiments. Over 50 cells were counted in each experiment. One-way analysis of variance with Tukey's *post hoc* test: *, $P < 0.005$ compared to the colocalization of LRRK1 and lysosome (E) or that of LRRK1 and VAMP7. (G) Assays of binding between different mutant LRRK1 proteins and VAMP7. Different mutant LRRK1-FLAG proteins and VAMP7-HA were transfected into HEK293 cells, and lysates were immunoprecipitated (IP) with antibodies against the proteins indicated at the top. Precipitated proteins were subjected to SDS-PAGE, and the blots were stained with antibodies against the target proteins indicated to the right.

LRRK1 is recruited to lysosomes by VAMP7. To explore the potential role of LRRK1 in endosome-lysosome fusion, we examined the intracellular localization of this protein (Fig. 3A and B). In *Lrrk1*$^{+/+}$ MEFs under physiological conditions, LRRK1 was distributed diffusely throughout the cytoplasm. Upon tunicamycin treatment, however, LRRK1 accumulated in autophagosomes labeled with LC3, suggesting that LRRK1 was recruited into autophagosomes during autophagy. We sought to determine which region of LRRK1 is responsible for the recruitment of LRRK1 to endosomal structures by monitoring the localization of various deletion mutant forms of LRRK1 in transfected MEFs (Fig. 3C to F). LRRK1-D1 and LRRK1-D2 were localized in lysosomes, whereas LRRK1-D3 and LRRK1-D4 were not (Fig. 3D and E). Thus, the N-terminal region of LRRK1, which contains ankyrin repeats and leucine-rich repeats, was required for the localization of LRRK1 to the lysosome. The ankyrin repeats and leucine-rich

repeats are involved in protein-protein interactions (37, 38), suggesting that the N-terminal region of LRRK1 is recruited to the lysosome by interacting molecules. Yeast two-hybrid screening with the N-terminal region of LRRK1 such as LRRK1-D1 identified VAMP7 as a molecule that interacts with this region. VAMP7 is one of the vesicular SNAREs, proteins that catalyze the fusion of two membranes of intracellular organelles (39, 40). By binding to cargo-specific proteins, VAMP7 localizes in the late endosome and lysosome in most cell types, and it is involved in endosomal trafficking from the late endosome to the lysosome or the Golgi apparatus. In MEFs expressing VAMP7 and mutant LRRK1, VAMP7 colocalized with LRRK1, LRRK1-D1, and LRRK1-D2 but not LRRK1-D3 or LRRK1-D4 (Fig. 3D and E). Coimmunoprecipitation and immunoblotting experiments confirmed that the N-terminal region of LRRK1 associated with VAMP7 (Fig. 3G).

In MEFs expressing LRRK1 and VAMP7, tunicamycin treatment induced LRRK1 accumulation at VAMP7-positive vesicles fused with VAMP7-positive lysosomes (Fig. 4A and B). Coimmunoprecipitation and immunoblotting experiments showed the association between endogenous LRRK1 and VAMP7, the intensity of which increased after tunicamycin treatment and decreased in the presence of LRRK1-D1 (Fig. 4C). We further analyzed the interaction between LRRK1 and VAMP7 by using a complementation reporter system with a coral fluorescent reporter protein (mKG) (41) (Fig. 4D). In MEFs transfected with the N-terminal region of LRRK1 fused to one portion of divided mKG and VAMP7 fused with the other portion, tunicamycin treatment resulted in a GFP signal. These results indicated that tunicamycin-induced autophagy induced the association between LRRK1 and VAMP7. On the other hand, MEFs expressing VAMP7 shRNA exhibited a less intimate association of LRRK1 with LC3 during tunicamycin-induced autophagy (Fig. 4E to G). Notably, the fusion of LC3-positive vesicles with lysosomes was also blocked in MEFs transfected with VAMP7 shRNA (Fig. 4F, arrowhead), consistent with the evidence that VAMP7 is required for endosome-lysosome fusion. Furthermore, overexpression of N-terminal LRRK1 (LRRK1-D1), exerting the dominant negative effect on the interaction between LRRK1 and VAMP7 (Fig. 4C), increased the enlarged LC3-positive vesicles in both *Lrrk1*$^{+/+}$ and *Lrrk1*$^{-/-}$ MEFs (data not shown). Thus, the recruitment of LRRK1 to lysosomes through VAMP7 is required for tunicamycin-induced autophagy.

LRRK1 regulates TBC1D2, a Rab7 GAP, and ARHGAP22, a Rac1 GAP. Next, we asked how LRRK1 regulates autophagosome-lysosome fusion. Rab7 is required for normal progression of autophagic flux (7, 42, 43). Hence, we monitored Rab7-GTP levels in *Lrrk1*$^{-/-}$ MEFs under starvation conditions or tunicamycin treatment (Fig. 5A and B). *Lrrk1*$^{+/+}$ MEFs exhibited elevated levels of Rab7-GTP following tunicamycin treatment, indicating that Rab7 activation allows autophagosome-lysosome fusion. In contrast, *Lrrk1*$^{-/-}$ MEFs had higher levels of Rab7-GTP under control conditions and further elevated Rab7-GTP levels under tunicamycin treatment. The introduction of LRRK1 but not kinase-dead LRRK1(D1386A) into *Lrrk1*$^{-/-}$ MEFs rescued the higher levels of Rab7-GTP. These results suggested that Rab7 inactivation, a step required for the release of Rab7 from donor vesicles and lysosome fusion, is mediated by LRRK1 through its kinase activity.

A recent report showed that Rac1 is inactivated during autophagy (44). *Lrrk1*$^{+/+}$ MEFs had reduced levels of Rac1-GTP under tunicamycin treatment (Fig. 5C and D), whereas *Lrrk1*$^{-/-}$ MEFs had higher Rac1-GTP levels than under control conditions or tunicamycin treatment. The introduction of LRRK1 but not kinase-dead LRRK1(D1386A) into *Lrrk1*$^{-/-}$ MEFs rescued the higher levels of Rac1-GTP. These results suggested that Rac1-GTP/GDP cycling during tunicamycin-induced autophagy is mediated by LRRK1 through its kinase activity. Thus, *Lrrk1* deletion reduced the GAP activity for both Rab7 and Rac1 in MEFs.

Sequence analysis revealed that the GAP consensus motif is absent from LRRK1 (45). Therefore, we hypothesized that LRRK1 regulates GAP activity via unknown molecules. Yeast two-hybrid screening with the C-terminal region such as LRRK1-D4, containing the kinase domain of LRRK1, identified TBC/RabGAP (TBC1D2) and ARHGAP22 as molecules that interact with this region. TBC1D2 and ARHGAP22 have similar domain structures; each contains a pleckstrin homology (PH) domain and a GAP domain, followed by a coiled-coil domain. ARHGAP22 inactivates Rac1 (46); TBC1D2 specifically inactivates Rab7 (44, 47) and is also an effector of Rac1 (47). Coimmunoprecipitation and immunoblotting experiments with transfected cells confirmed that the C-terminal region of LRRK1 (LRRK1-D4) associated with TBC1D2 and ARHGAP22 (Fig. 5E). Coimmunoprecipitation and immunoblotting experiments with MEFs showed the association between endogenous LRRK1 and TBC1D2 or ARHGAP22, the intensity of which increased after tunicamycin treatment and decreased in the presence of LRRK1-D4 (Fig. 5F and G). These results indicated that tunicamycin-mediated autophagy increased the association between LRRK1 and TBC1D2 or ARHGAP22. To determine whether a defect in autophagosome-lysosome fusion is caused by dysfunction of TBC1D2 or ARHGAP22, we subjected MEFs lacking TBC1D2 or ARHGAP22 to tunicamycin treatment (Fig. 5H to J). MEFs transfected with TBC1D2 shRNA contained higher LC3 levels, whereas MEFs transfected with ARHGAP22 shRNA exhibited no detectable changes in LC3 compared with *Lrrk1*$^{+/+}$ MEFs (Fig. 5H and I).

Lrrk1$^{+/+}$ MEFs transfected with TBC1D2 shRNA contained enlarged autophagosomes, whereas *Lrrk1*$^{-/-}$ MEFs transfected with ARHGAP22 shRNA exhibited no detectable changes in autophagosomes (Fig. 6A and B). Furthermore, the overexpression of C-terminal LRRK1 (LRRK1-D4), showing the dominant negative effect on the interaction between LRRK1 and TBC1D2 (Fig. 5F), increased the enlarged LC3-positive vesicles in both *Lrrk1*$^{+/+}$ MEFs and *Lrrk1*$^{-/-}$ MEFs (data not shown). Thus, TBC1D2 could be a major player in autophagosome-lysosome fusion, although ARHGAP22 might regulate the autophagic pathway by inactivating Rac1. To investigate this possibility, we examined the autophagic pathway in MEFs transfected with GFP/mCherry-LC3 and mutant Rab7 (Fig. 6C to E). *Lrrk1*$^{+/+}$ MEFs expressing dominant negative Rab7T22N contained enlarged LC3-positive vesicles that were not colocalized with lysosomes (arrowheads), suggesting that Rab7T22N blocked autophagosome-lysosome fusion, leading to the accumulation of unfused autophagosomes. In contrast, *Lrrk1*$^{+/+}$ MEFs expressing constitutively active Rab7Q67L contained enlarged LC3-positive vesicles that were colocalized with lysosomes (arrows), suggesting that Rab7Q67L blocked the autophagosome degradation process after fusion, leading to the accumulation of undegraded autophagosomes. Thus, overactivation of Rab7 disturbed autophagosome-lysosome fusion, resulting in changes similar to those observed in *Lrrk1*$^{-/-}$ MEFs. Next, we studied whether the tunicamycin-induced morphological changes in *Lrrk1*$^{-/-}$ MEFs are due to the excess of Rab7 activity. In

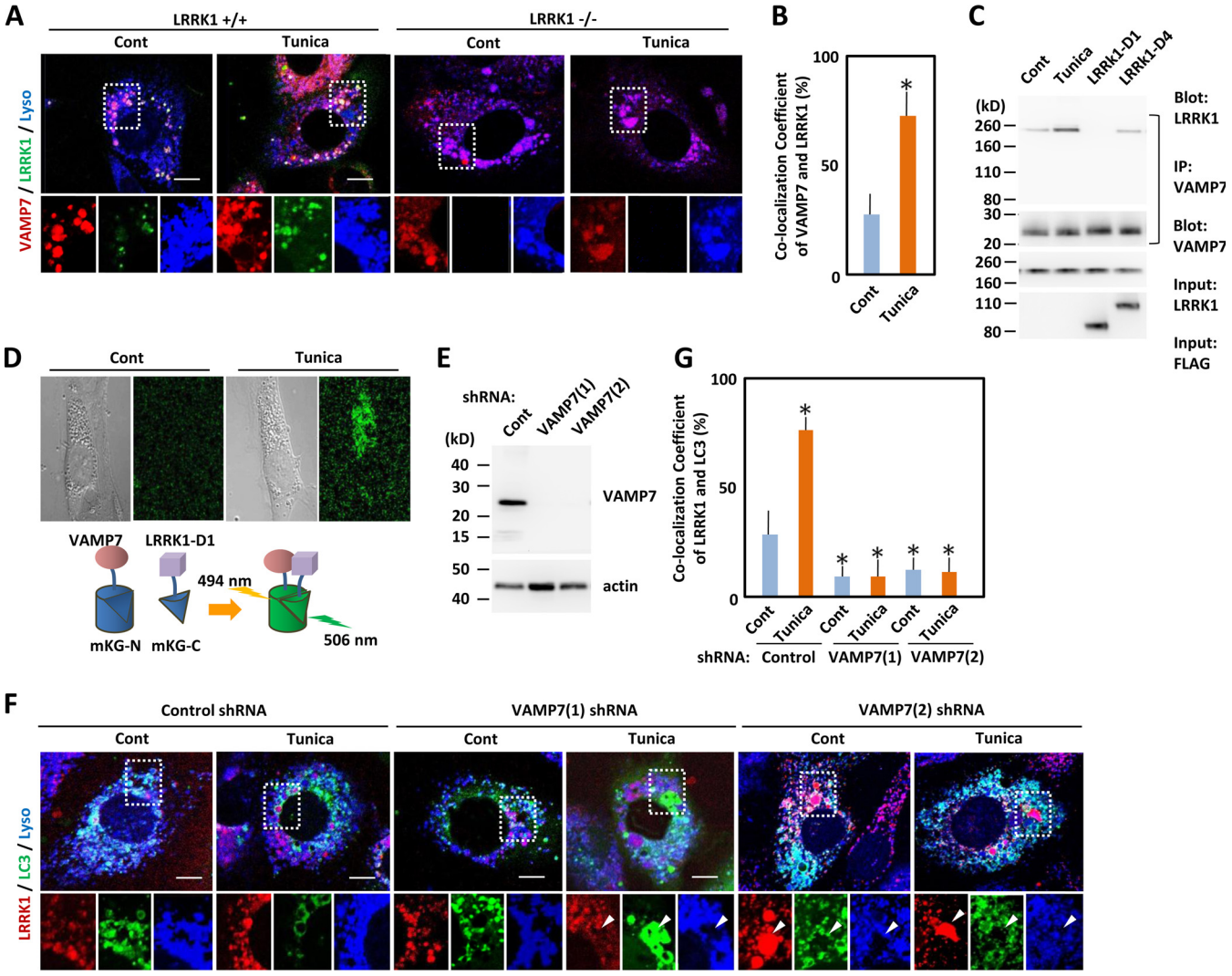

FIG 4 LRRK1 is recruited to lysosomes by VAMP7. (A) *Lrrk1*$^{+/+}$ MEFs expressing LRRK1-GFP and VAMP7-Red were treated with the control (Cont) or tunicamycin (Tunica) for 4 h and stained with LysoTracker for last 30 min. Merged images of MEFs (top) and magnified images of the boxed areas (bottom) are shown. Scale bars, 10 μm. (B) Immunofluorescence colocalization of mutant forms of LRRK1-GFP and VAMP7-Red expressed in *Lrrk1*$^{+/+}$ MEFs. The colocalization of two proteins was analyzed by Pearson and Spearman correlation coefficients. The error bars represent standard deviations from three independent experiments. Over 50 cells were counted in each experiment. One-way analysis of variance with Tukey's *post hoc* test: *, $P < 0.005$ compared to control *Lrrk1*$^{+/+}$ MEFs. (C) Binding assay to detect the association between endogenous LRRK1 and VAMP7. MEFs were treated with tunicamycin or transfected with LRRK1-D1 or LRRK1-D4 and lysed. Lysates were immunoprecipitated (IP) with anti-VAMP7 antibodies. Precipitated proteins were subjected to SDS-PAGE, and the blots were stained with anti-LRRK1 antibodies or anti-VAMP7 antibodies. (D) Detection of protein-protein interactions with the mKG reporter system in transfected *Lrrk1*$^{+/+}$ MEFs. Cells expressed mKG-C fused to the N terminus of LRRK1-D1 and mKG-N fused to VAMP7. Transfected cells exhibited faint mKG fluorescence under control conditions but increased fluorescence under tunicamycin treatment (Tunica), reflecting the tunicamycin-induced interaction between VAMP7 and LRRK1-D1. (E) Expression of endogenous VAMP7 in MEFs. MEFs were transfected with an shRNA vector containing a scrambled oligonucleotide (control shRNA) or an shRNA vector containing oligonucleotides against different sequences of VAMP7 [VAMP7(1) or VAMP7(2) shRNA]. Transfected cells were lysed. Lysates were subjected to SDS-PAGE, and the blots were immunoblotted with anti-VAMP7 antibodies. (F) *Lrrk1*$^{+/+}$ MEFs expressing GFP/mCherry-LC3 and LRRK1-Red were transfected with control, VAMP7(1), or VAMP7(2) shRNA. Cells were treated with the control (Cont) or tunicamycin (Tunica) for 4 h and stained with LysoTracker for last 30 min. Merged images of MEFs (top) and magnified images of the boxed areas (bottom) are shown. Scale bars, 10 μm; arrowheads indicate the LRRK1-positive vesicles not fused with lysosomes. (G) Immunofluorescence colocalization of GFP-LC3 and LRRK1-Red expressed in *Lrrk1*$^{+/+}$ MEFs. The colocalization of two proteins was analyzed by Pearson and Spearman correlation coefficients. The error bars represent standard deviations from three independent experiments. Over 50 cells were counted in each experiment. One-way analysis of variance with Tukey's *post hoc* test: *, $P < 0.005$ compared to control *Lrrk1*$^{+/+}$ MEFs transfected with control shRNA.

response to tunicamycin, *Lrrk1*$^{-/-}$ MEFs expressing Rab7T22N or Rab7 shRNA contained smaller LC3-positive vesicles that were not colocalized with lysosomes (arrowheads), suggesting that suppression of Rab7 activity partially rescues the enlarged LC3-positive vesicles. These findings agree with previous findings that the decreased autophagic pathway is correlated with reductions in the Rab7-GAP activity of TBC1D2 (44). Collectively, these data suggest that TBC1D2-mediated Rab7 inactivation is involved in LRRK1-mediated endosome-lysosome fusion during tunicamycin-induced autophagy.

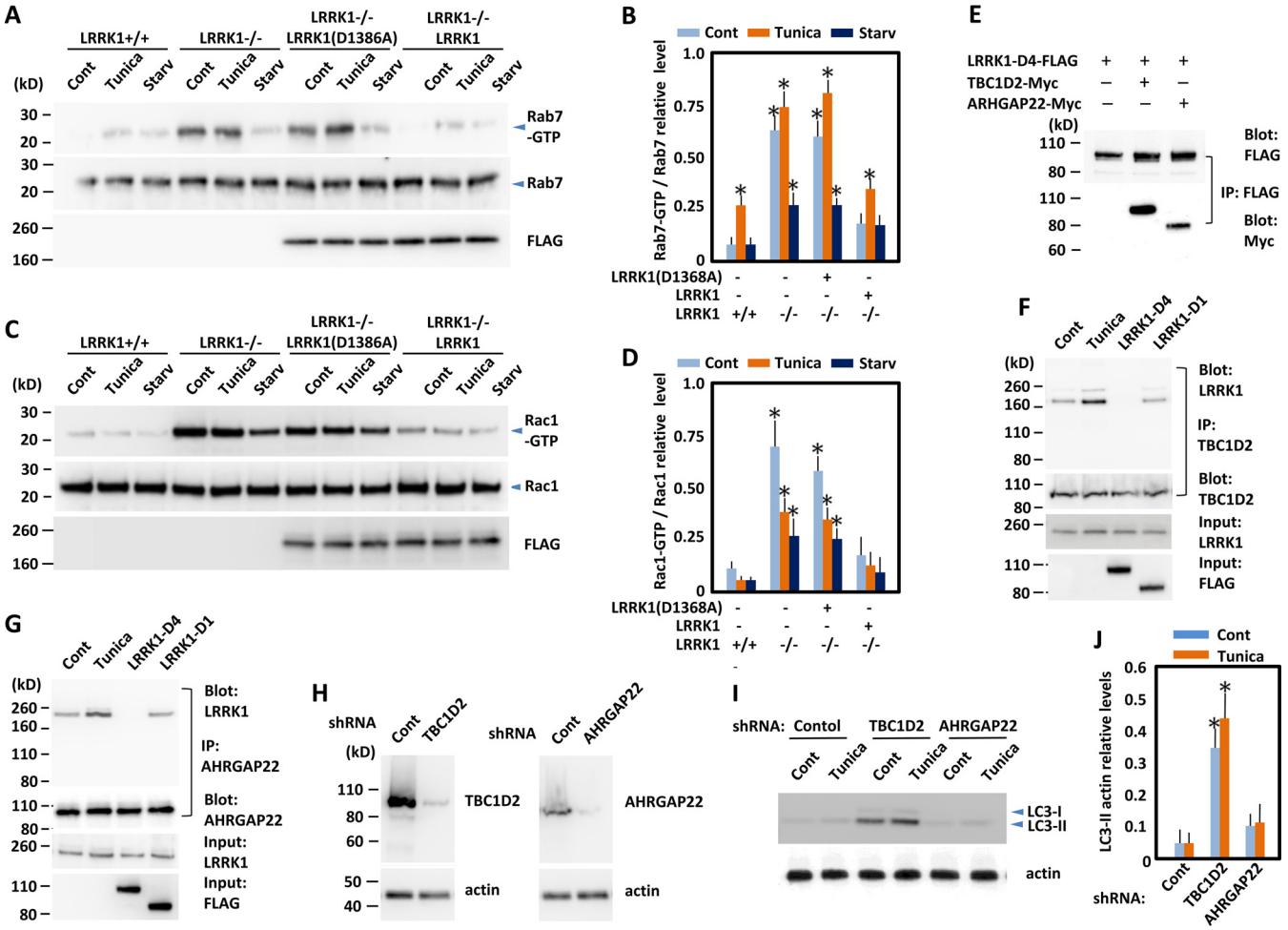

FIG 5 LRRK1 regulates Rab7 and Rac1 activities through TBC1D2 and AHRGAP22. (A) *Lrrk1*$^{+/+}$ and *Lrrk1*$^{-/-}$ MEFs with or without wild-type or kinase-dead LRRK1 [LRRK1(D1368A)] were treated under control (Cont), tunicamycin (Tunica), or starvation (Starv) conditions for 2 h. Lysates were processed for detection of Rab7-GTP with an anti-Rab7-GTP antibody. Total Rab7 was detected with an anti-Rab7 antibody. (B) Values were normalized against Rab7 levels. The error bars represent standard deviations from three independent experiments. One-way analysis of variance with Tukey's *post hoc* test: *, $P < 0.05$ compared to control *Lrrk1*$^{+/+}$ MEFs. (C) *Lrrk1*$^{+/+}$ and *Lrrk1*$^{-/-}$ MEFs with or without wild-type or kinase-dead LRRK1 [LRRK1(D1368A)] were treated under control, tunicamycin, or starvation conditions for 2 h. Lysates were processed for detection of Rac1-GTP with the PAK-1 PBD. Total Rac1 was detected with an anti-Rac1 antibody. (D) Values were normalized against Rac1 levels. The error bars represent standard deviations from three independent experiments. One-way analysis of variance with Tukey's *post hoc* test: *, $P < 0.05$ compared to control *Lrrk1*$^{+/+}$ MEFs. (E) Binding assays to detect interactions between LRRK1-D4 and TBC1D2 or ARHGAP22. LRRK1-D4 and TBC1D2 or ARHGAP22 were transfected into HEK293 cells, and lysates were immunoprecipitated (IP) with anti-FLAG antibodies. Precipitated proteins were subjected to SDS-PAGE, and the blots were stained with anti-FLAG or anti-Myc antibodies. (F) Binding assays to detect interactions between endogenous LRRK1 and TBC1D2. MEFs were treated with tunicamycin or transfected with LRRK1-D4 or LRRK1-D1 and lysed. Lysates were immunoprecipitated with anti-TBC1D2 antibodies. Precipitated proteins were subjected to SDS-PAGE, and the blots were stained with anti-LRRK1 or anti-TBC1D2 antibodies. (F) Binding assays to detect interactions between endogenous LRRK1 and ARHGAP22. MEFs were treated with tunicamycin or transfected with LRRK1-D4 or LRRK1-D1 and lysed. Lysates were immunoprecipitated with anti-ARHGAP22 antibodies. Precipitated proteins were subjected to SDS-PAGE, and the blots were stained with anti-LRRK1 or anti-ARHGAP22 antibodies. (H) Expression of endogenous TBC1D2 or AHRGAP22 in MEFs. MEFs were transfected with an shRNA vector containing a scrambled oligonucleotide (control shRNA) or an shRNA vector containing an oligonucleotide against TBC1D2 (TBC1D2 shRNA) or ARHGAP22 (ARHGAP22 shRNA). Transfected cells were lysed. Lysates were subjected to SDS-PAGE, and the blots were immunoblotted with anti-TBC1D2 or anti-ARHGAP antibodies. (I) Immunoblotting of LC3. *Lrrk1*$^{+/+}$ MEFs transfected with control, TBC1D2, or AHRGAP22 shRNA were treated with the control or tunicamycin, and endogenous LC3 levels were measured by blot analysis. (J) Values were normalized against actin levels. The error bars represent standard deviations from three independent experiments. One-way analysis of variance with Tukey's *post hoc* test: *, $P < 0.005$ compared to control *Lrrk1*$^{+/+}$ MEFs.

LRRK1 regulates autophagy by activating TBC1D GAP activity. The intramolecular association between the PH and GAP domains suppresses the GAP activity of Ras/p120 GAP (48). TBC1D2 has structural features in common with p120 GAP, suggesting that the Rab7-GAP activity of TBC1D2 is regulated by intramolecular association between the PH and TBC (Tre-2/Bub2/Cdc16) domains. To investigate this possibility, we generated TBC1D2 deletion constructs lacking the PH domain (ΔPH-TBC) and the TBC domain (ΔTBC-TBC) and transfected them into *Lrrk1*$^{-/-}$ MEFs (Fig. 7A). Coimmunoprecipitation and immunoblotting revealed that the PH domain bound to the TBC domain in the absence of LRRK1 but less strongly in the presence of LRRK1 (Fig. 7B), suggesting that association between the PH domain and the TBC domain occurs but is suppressed by LRRK1.

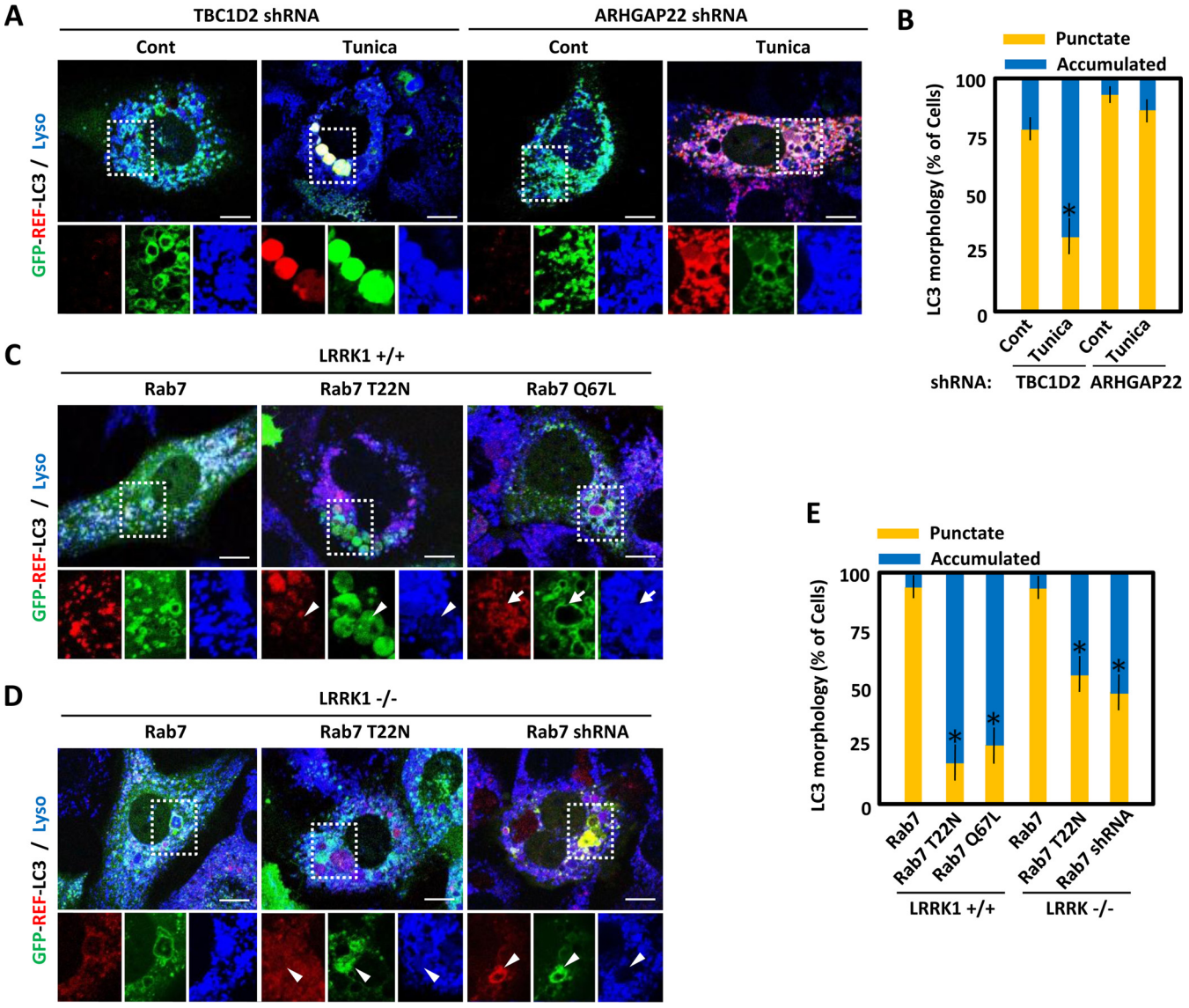

FIG 6 LRRK1 regulates autophagosome-lysosome fusion through TBC1D2-mediated Rab7. (A) *Lrrk1*$^{+/+}$ MEFs expressing GFP/mCherry-LC3 were transfected with an shRNA vector targeting TBC1D2 (TBC1D2 shRNA) or ARHGAP22 (ARHGAP22 shRNA). Cells were treated with the control (Cont) or tunicamycin (Tunica) for 4 h and stained with LysoTracker for the last 30 min. Merged images of MEFs (top) and magnified images of the boxed areas (bottom) are shown. Scale bars, 10 μm. (B) Percentages of cells harboring punctate or accumulated GFP/mCherry-LC3 are shown. Criteria for LC3 morphology are outlined in Fig. 2A. The error bars represent standard deviations from three independent experiments. Over 50 cells were counted in each experiment. One-way analysis of variance with Tukey's *post hoc* test: *, $P < 0.005$ compared to *Lrrk1*$^{+/+}$ MEFs transfected with control shRNA. (C) *Lrrk1*$^{+/+}$ or *Lrrk1*$^{-/-}$ MEFs expressing different mutant Rab7 proteins or shRNA were stained with LysoTracker for 30 min. (D) Merged images of MEFs (top) and magnified images of the boxed areas (bottom) are shown. Scale bars, 10 μm. (C and D) Arrows indicate LC3-positive vesicles fused with lysosomes, and arrowheads indicate LC3-positive vesicles not fused with lysosomes. (E) Percentages of cells harboring punctate or accumulated GFP/mCherry-LC3 are shown. Criteria for LC3 morphology are outlined in Fig. 2A. The error bars represent standard deviations from three independent experiments. Over 50 cells were counted in each experiment. One-way analysis of variance with Tukey's *post hoc* test: *, $P < 0.005$ compared to *Lrrk1*$^{+/+}$ MEFs transfected with control shRNA.

In addition, MEFs expressing ΔPH-TBC exhibited reduced Rab7-GTP levels under control conditions and tunicamycin treatment (Fig. 7C and D), suggesting that the TBC domain enhanced the protein's Rab7-GAP activity, whereas MEFs expressing ΔTBC-TBC exhibited elevated Rab7-GTP levels, suggesting that the PH domain blocked the Rab7-GAP activity of endogenous TBC1D2. Consistent with these results, the introduction of ΔPH-TBC into *Lrrk1*$^{-/-}$ MEFs decreased elevated Rab7-GTP levels, whereas that of ΔTBC-TBC enhanced Rab7-GTP levels (Fig. 7C and D). Thus, one model of the mode of TBC1D2 action is that in the absence of LRRK1, the PH domain can interact with the TBC domain, leading to the inhibition of GAP activity; in contrast, in the presence of LRRK1, the PH domain is detached from the TBC domain, leading to GAP activation. Such a model implies that LRRK1 may cause a switch in GAP activity by regulating intramolecular contact between the PH and TBC domains of TBC1D2 (Fig. 7E).

In the context of Rab7 regulation, ΔPH-TBC functions as a constitutively active form of TBC1D2 and ΔTBC-TBC functions

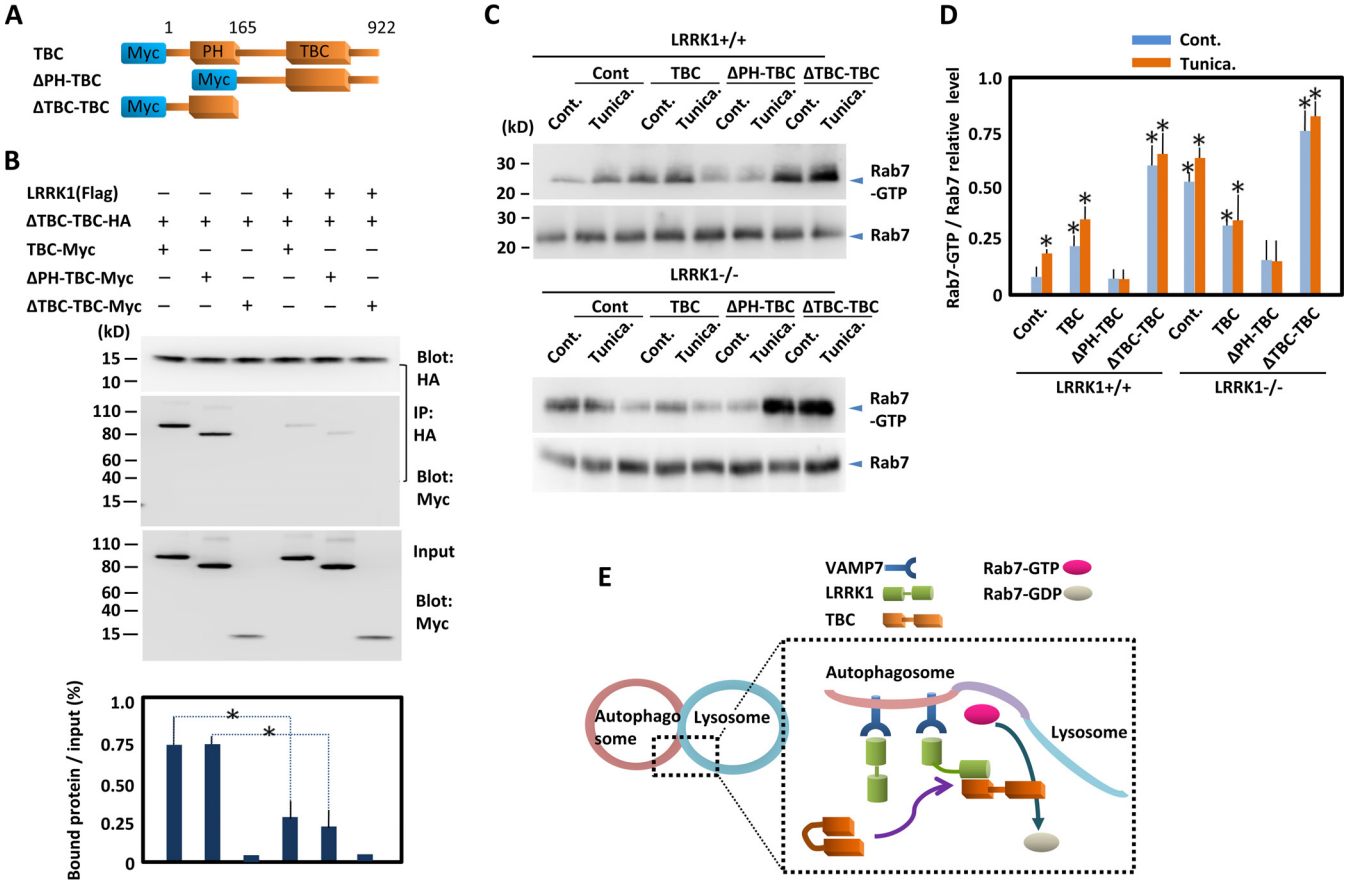

FIG 7 LRRK1 regulates the intramolecular interaction of TBC1D2. (A) Diagram showing full-length and truncated TBC1D2. Amino acids are noted at the top. (B) Binding assays to detect interactions between various TBC1D2 domains and the PH domain. Various mutant TBC1D2-Myc proteins and ΔTBC-TBC-HA were transfected into HEK293 cells, and lysates were immunoprecipitated (IP) with an antibody against the HA epitope. Precipitated proteins were subjected to SDS-PAGE, and the blots were stained with an antibody against HA or Myc epitopes, as indicated to the right. The ratio of bound/total protein is shown at the bottom. The error bars represent standard deviations from three independent experiments. Paired *t* test: *, $P < 0.005$ between the pairs indicated. (C) *Lrrk1*$^{+/+}$ or *Lrrk1*$^{-/-}$ MEFs were transfected with mutant TBC constructs. Cells were treated with the control (Cont) or tunicamycin (Tunica) for 2 h. Lysates were processed to detect Rab7-GTP with an anti-Rab7-GTP antibody. Total Rab7 was detected with an anti-Rab7 antibody. (D) Levels of Rab7-GTP were calculated relative to levels of total Rab7. The error bars represent standard deviations from three independent experiments. One-way analysis of variance with Tukey's *post hoc* test: *, $P < 0.05$ compared to *Lrrk1*$^{+/+}$ MEFs transfected with control shRNA. (E) Working model of LRRK1 function in autophagosome-lysosome fusion. Upon autophagy, LRRK1 binds to the autophagosome through VAMP7 and is transferred to the lysosome. LRRK1 localization at autolysosomes enables the activation of the Rab7-GAP activity of TBC1D2 via interaction with the PH domain and reconfiguration of the TBC domain.

as a dominant negative form. To test the possibility that LRRK1-mediated autophagic flux is regulated by the Rab7-GAP activity of TBC1D2, we subjected MEFs expressing truncated TBC to tunicamycin treatment. The LC3-II levels in *Lrrk1*$^{+/+}$ MEFs were augmented by overexpression of ΔTBC-TBC (Fig. 8A and B), whereas in *Lrrk1*$^{-/-}$ MEFs, the LC3-II levels were suppressed by overexpression of ΔPH-TBC but augmented by overexpression of ΔTBC-TBC (Fig. 8C and D). On the other hand, the LC3-II levels in both *Lrrk1*$^{+/+}$ and *Lrrk1*$^{-/-}$ MEFs were increased by Rab7 shRNA. Thus, the GTP/GDP cycling of Rab7 by LRRK1-dependent TBC1D2 GAP activity is required for autophagic flux. When MEFs expressing mutant TBC1D2 were transfected with GFP-mCherry-LC3, overexpression of ΔTBC-TBC increased the enlarged LC3-positive vesicles in *Lrrk1*$^{+/+}$ MEFs (Fig. 8E and F), whereas overexpression of ΔPH-TBC reduced the number of enlarged LC3-positive vesicles in *Lrrk1*$^{-/-}$ MEFs (Fig. 8E and F). Thus, LRRK1-mediated autophagic flux depended on the Rab7-GAP activity of TBC1D2. Together with the findings that LRRK1 suppressed the interaction between the PH and TBC domains, leading to Rab7-GAP activation, these observations led us to conclude that LRRK1 regulates the Rab7-GAP activity crucial for autophagic flux by dissociating the inhibitory PH domain from the catalytic TBC domain of TBC1D2.

DISCUSSION

Autophagy requires integration with intracellular trafficking and cytoskeletal remodeling. Multiple Rab proteins regulate different steps of autophagosome biogenesis, and each cycle of Rab activation and inactivation is precisely controlled. Both positive (guanine nucleotide exchange factors or GEFs) and negative (GAPs) regulators of Rab proteins define the timing, duration, and specificity of Rab signaling in each intracellular compartment (49). Rab7 promotes membrane fusion between the late endosome and lysosome, as well as between autophagosomes and lysosomes (6, 7).

In this study, we found that LRRK1 promotes Rab7 inactiva-

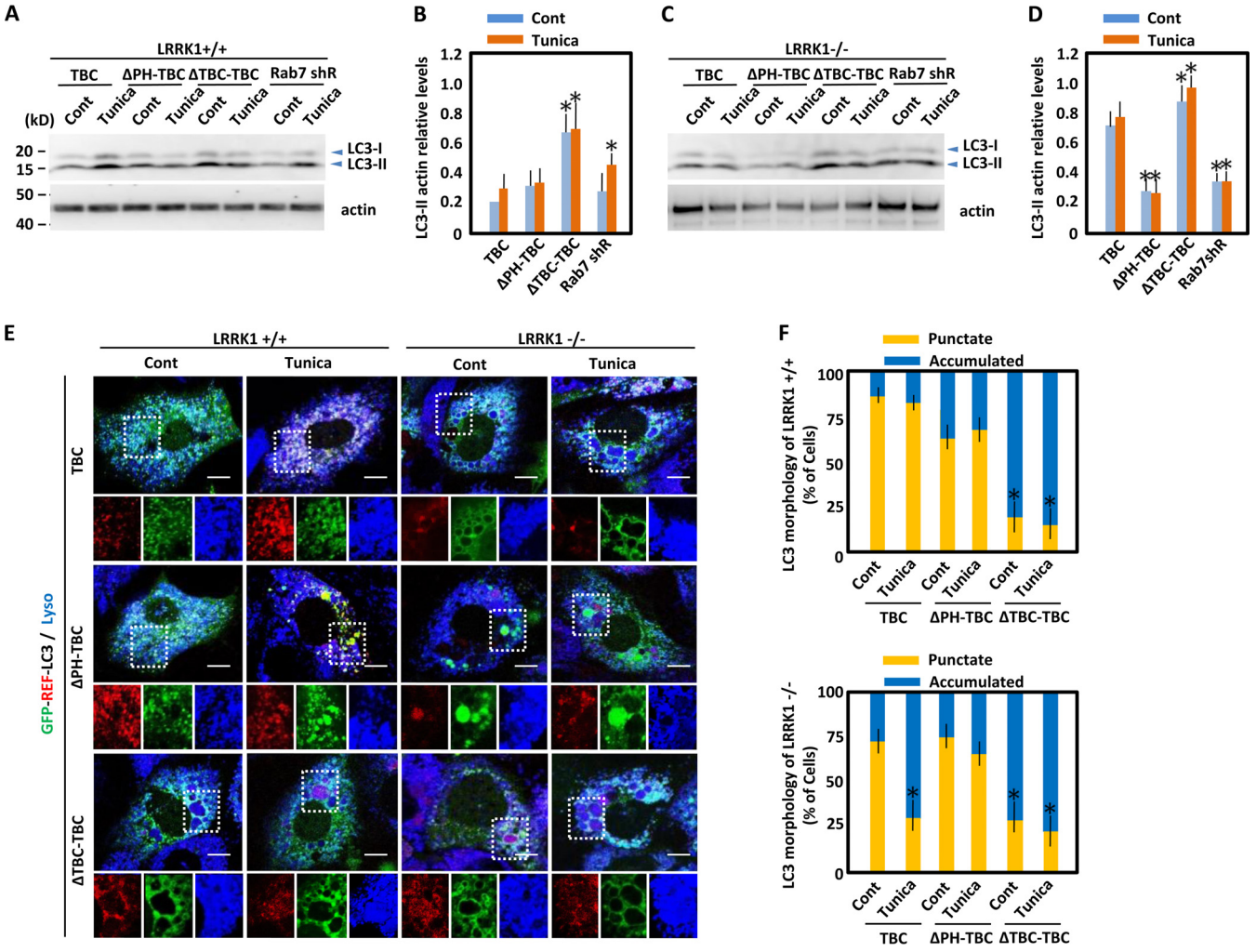

FIG 8 Constitutively active mutant TBC1D2 rescues the LC3 morphology in *Lrrk1*$^{+/+}$ MEFs. (A) Immunoblotting of LC3. *Lrrk1*$^{+/+}$ MEFs were transfected with mutant TBC constructs or Rab7 shRNA. Cells were treated with the control (Cont) or tunicamycin (Tunica), and endogenous LC3 levels were measured by blot analysis. (B) Values were normalized against actin levels. The error bars represent standard deviations from three independent experiments. One-way analysis of variance with Tukey's *post hoc* test: *, $P < 0.05$ compared to control *Lrrk1*$^{+/+}$ MEFs. (C) Immunoblotting of LC3. *Lrrk1*$^{-/-}$ MEFs transfected with mutant TBC constructs or Rab7 shRNA were treated with the control or tunicamycin, and endogenous LC3 levels were measured by blot analysis. (D) Values were normalized against actin levels. The error bars represent standard deviations from three independent experiments. One-way analysis of variance with Tukey's *post hoc* test: *, $P < 0.05$ compared to control *Lrrk1*$^{-/-}$ MEFs. (E) *Lrrk1*$^{+/+}$ and *Lrrk1*$^{-/-}$ MEFs expressing GFP/mCherry-LC3 transfected with mutant TBC constructs were treated with the control or tunicamycin for 4 h and stained with LysoTracker for last 30 min. Merged images of MEFs (top) and magnified images of the boxed areas (bottom) are shown. Scale bars, 10 μm. (F) Percentages of cells harboring punctate or accumulated GFP/mCherry-LC3 are shown. Criteria for LC3 morphology are outlined in Fig. 2A. The error bars represent standard deviations from three independent experiments. Over 50 cells were counted in each experiment. One-way analysis of variance with Tukey's *post hoc* test: *, $P < 0.005$ compared to *Lrrk1*$^{+/+}$ (top) or *Lrrk1*$^{-/-}$ (bottom) MEFs transfected with TBC1D2.

tion during lysosomal fusion by activating a Rab7 GAP, TBC1D2. The disrupted Rab7 inactivation in *Lrrk1*$^{-/-}$ cells has several physiological implications. The primary defect is reduced delivery of endocytic and autophagic components to lysosomes, leading to a reduced capacity to degrade lipids and proteins. Consequently, digestion and autophagy are compromised and the cell is unable to use its own cytoplasm to provide nutrients. Indeed, *Lrrk1*$^{-/-}$ mice have much more difficulty surviving starvation after birth. Our biochemical analysis of *Lrrk1*$^{-/-}$ mice also identified reduced clearance of autophagy-induced LC3-II, resulting from a defect in autophagosome-lysosome fusion, and lower activity of lysosomal enzymes, due to defects in lysosomal enzyme-containing endosome-lysosome fusion, which is proposed to be controlled by Rab7 (6, 7).

One mechanism of Rab7 inactivation by LRRK1 requires the strategic localization of LRRK1 to lysosomes, enabling LRRK1 to associate with TBC1D2. Screening for molecules that interact with the N-terminal region of LRRK1, which is responsible for the protein's lysosomal localization, identified the SNARE VAMP7. A fluorescent-reporter assay confirmed the colocalization of LRRK1 and VAMP7 in lysosomes during tunicamycin-induced autophagy. Indeed, LRRK1 lacking the VAMP7-interacting N-terminal region does not localize to the lysosome, whereas VAMP7 deletion by shRNA prevents LRRK1 from localizing to the lyso-

some. Together with the correct localization of VAMP7 in *Lrrk1*$^{-/-}$ cells, the recruitment of LRRK1 depends on the sorting of VAMP7 in endosomal trafficking. There are 36 SNAREs in humans, each of which must be sorted to its own specific target membrane (39, 40). VAMP7 is sorted to the late endosome/lysosome via direct binding to a clathrin adaptor protein, AP3 (50), or Hrb, an ArfGAP (51). All lysosomal fusion events require VAMP7 (40). Thus, it is plausible that VAMP7 can drive the recruitment of LRRK1 to lysosomes during tunicamycin-induced autophagy.

The second mechanism of Rab7 inactivation by LRRK1 requires the activation of TBC1D2. Rab7 is required for autophagic flux (7, 42, 43). LRRK1 deletion induced accumulation of autophagosomes, concomitant with high levels of Rab7-GTP. Either dominant negative Rab7T22N or constitutively active Rab7Q67L induced enlarged autolysosomes, suggesting that Rab7-GTP/GDP cycling is essential for autophagic flux. Furthermore, ΔPH-TBC, which promoted Rab7GTP/GDP conversion, effectively decreased the amount of LC3-II to control levels and inhibited the formation of enlarged autophagosomes during tunicamycin-induced autophagy in *Lrrk1*$^{-/-}$ MEFs. Thus, defects in autophagic flux in *Lrrk1*$^{-/-}$ MEFs could be due to reduced Rab7 inactivation.

Various TBC-containing Rab GAPs interact with LC3 and may integrate autophagy with intracellular trafficking (52, 53). TBC1D2, which localizes in the endosome and autophagosome via an interaction with LC3, specifically inactivates Rab7 (44, 47). This interaction with LC3 is competitively blocked by Rac1-GTP, which is inactivated during tunicamycin-induced autophagy (44). *Lrrk1*$^{-/-}$ MEFs contained higher levels of Rac1, as well as Rab7, during tunicamycin-induced autophagy (Fig. 5A and B), suggesting inactivation of ARHGAP22, another LRRK1-interacting molecule, in these cells. Thus, high Rab7-GTP levels could result from the Rac1-GTP-mediated block of TBC1D2-LC3 interaction. However, ARHGAP22 deletion had no detectable effects on LC3 levels or autolysosome morphology (Fig. 5D and E). Alternatively, intramolecular folding between the PH domain and the GAP domain may regulate the GAP activity in p120 GAP (48). Indeed, the PH domain bound to the GAP domain and increased the level of Rab7-GTP because of the suppression of Rab7 GAP, and this suppression was alleviated by the overexpression of LRRK1. Accordingly, we propose a model in which LRRK1 regulates Rab7 GAP of TBC1D2. In this model, the PH domain of TBC1D2 binds to the catalytic TBC domain, keeping the protein folded upon itself. LRRK1 binding to the PH domain displaces the PH domain from the TBC domain, exposing the catalytic region of the TBC domain and allowing it to interact with Rab7.

Together, these data support a model that serves as the mechanism of sustained autophagic flux. The autophagosome initially moves and fuses with the lysosome via the HOPS complex in conjunction with Rab7-GTP (7, 8). Concomitantly, LRRK1 is recruited to the autophagosome via direct binding to VAMP7, an interaction that enables LRRK1 to bind TBC1D2 and activates its Rab7-GAP activity. LRRK1-positive autolysosomes then convert Rab7-GTP to Rab7-GDP, resulting in the dissociation of the HOPS complex from autolysosomes. The effective conversion of Rab7-GTP/GDP recycles Rab7-GDP to the Rab7 activation step for reuse in the autophagosome-lysosome fusions. Of note, the LRRK1 homologue LRRK2, a protein related to Parkinson's disease, is involved in autophagy (16, 18, 19) and Rab7 cycling (22, 23, 54). In contrast to the role of LRRK1 in autophagosome biogenesis, deletion or pathogenic mutation of LRRK2 causes a defect in autophagosome maturation, as revealed by the reduced conversion of LC3-I to LC3-II during autophagy (16, 18, 19). This defect could be explained by disrupted Rab7 activation (22, 23, 54). Although the molecular mechanism by which Rab7-GTP is induced in the late endosome remains controversial (55–57), it is clear that LRRK2 binds to Rab7L1-GTP and that the defect in endolysosomal and Golgi apparatus sorting caused by pathogenic LRRK2 is rescued by constitutively active Rab7L1 (23, 54). Thus, LRRK2 is involved in Rab7 activation during autophagy.

Together, these data indicate that LRRK1 and LRRK2 regulate the respective steps of Rab7 activation-inactivation cycling in order to promote autophagic flux. Phylogenetic analysis showed that LRRK2 originated from a gene duplication and that *Drosophila* contains a single LRRK-encoding gene (58). The *Drosophila* LRRK protein is structurally much more similar to LRRK1 than to LRRK2. Indeed, a mutant form of *Drosophila* LRRK analogous to the pathogenic LRRK2(G2019S) allele promoted rather than inhibited Rab7-dependent lysosome perinuclear clustering in *Drosophila* cells (59). The enhanced effect of pathogenic *Drosophila* LRRK on Rab7 activity is consistent with that of LRRK1 observed in this study. Thus, *Drosophila* LRRK is genetically closer to mammalian LRRK1 and may not be a good model for understanding human LRRK2 function. Under pathological conditions caused by LRRK2 mutation, such as Parkinson's disease, a functional defect in Rab7 activation could be compensated for by LRRK1. These data should facilitate the development of novel therapies against LRRK2-related Parkinson's disease

ACKNOWLEDGMENTS

This study was supported by research grants from the Ministry of Education, Culture, Sports, Science and Technology of Japan (T.T. and A.K.); a grant-in-aid from the Ministry of Health, Labor and Welfare (A.K.); the Founding Program for Next Generation World-Leading Researchers (NEXT Program); and special Coordination Funds for Promoting Science and Technology (A.K.). We have no conflicting financial interest.

T.T. and A.K. designed the experiments, all of us performed the experiments, and T.T. prepared the manuscript.

REFERENCES

1. **Tsukamoto S, Kuma A, Murakami M, Kishi C, Yamamoto A, Mizushima N.** 2008. Autophagy is essential for preimplantation development of mouse embryos. Science **321:**117–120. http://dx.doi.org/10.1126/science.1154822.
2. **Mizushima N, Levine B, Cuervo AM, Klionsky DJ.** 2008. Autophagy fights disease through cellular self-digestion. Nature **451:**1069–1075. http://dx.doi.org/10.1038/nature06639.
3. **Nakatogawa H, Ichimura Y, Ohsumi Y.** 2007. Atg8, a ubiquitin-like protein required for autophagosome formation, mediates membrane tethering and hemifusion. Cell **130:**165–178. http://dx.doi.org/10.1016/j.cell.2007.05.021.
4. **Tooze SA.** 2010. The role of membrane proteins in mammalian autophagy. Semin Cell Dev Biol **21:**677–682. http://dx.doi.org/10.1016/j.semcdb.2010.03.007.
5. **Levine B, Kroemer G.** 2008. Autophagy in the pathogenesis of disease. Cell **132:**27–42. http://dx.doi.org/10.1016/j.cell.2007.12.018.
6. **Hyttinen JM, Niittykoski M, Salminen A, Kaarniranta K.** 2013. Maturation of autophagosomes and endosomes: a key role for Rab7. Biochim Biophys Acta **1833:**503–510. http://dx.doi.org/10.1016/j.bbamcr.2012.11.018.
7. **Wang T, Ming Z, Xiaochun W, Hong W.** 2011. Rab7: role of its protein interaction cascades in endo-lysosomal traffic. Cell Signal **23:**516–521. http://dx.doi.org/10.1016/j.cellsig.2010.09.012.
8. **Balderhaar HJ, Ungermann C.** 2013. CORVET and HOPS tethering complexes—coordinators of endosome and lysosome fusion. J Cell Sci **126:**1307–1316. http://dx.doi.org/10.1242/jcs.107805.

9. **Bosgraaf L, Van Haastert PJ.** 2003. Roc, a Ras/GTPase domain in complex proteins. Biochim Biophys Acta **1643:**5–10. http://dx.doi.org/10.1016/j.bbamcr.2003.08.008.
10. **Ho CC, Rideout HJ, Ribe E, Troy CM, Dauer WT.** 2009. The Parkinson disease protein leucine-rich repeat kinase 2 transduces death signals via Fas-associated protein with death domain and caspase-8 in a cellular model of neurodegeneration. J Neurosci **29:**1011–1016. http://dx.doi.org/10.1523/JNEUROSCI.5175-08.2009.
11. **Imai Y, Gehrke S, Wang HQ, Takahashi R, Hasegawa K, Oota E, Lu B.** 2008. Phosphorylation of 4E-BP by LRRK2 affects the maintenance of dopaminergic neurons in Drosophila. EMBO J **27:**2432–2443. http://dx.doi.org/10.1038/emboj.2008.163.
12. **Gehrke S, Imai Y, Sokol N, Lu B.** 2010. Pathogenic LRRK2 negatively regulates microRNA-mediated translational repression. Nature **466:**637–641. http://dx.doi.org/10.1038/nature09191.
13. **Gandhi PN, Wang X, Zhu X, Chen SG, Wilson-Delfosse AL.** 2008. The Roc domain of leucine-rich repeat kinase 2 is sufficient for interaction with microtubules. J Neurosci Res **86:**1711–1720. http://dx.doi.org/10.1002/jnr.21622.
14. **Gillardon F.** 2009. Leucine-rich repeat kinase 2 phosphorylates brain tubulin-beta isoforms and modulates microtubule stability–a point of convergence in Parkinsonian neurodegeneration? J Neurochem **110:**1514–1522. http://dx.doi.org/10.1111/j.1471-4159.2009.06235.x.
15. **Piccoli G, Condliffe SB, Bauer M, Giesert F, Boldt K, De Astis S, Meixner A, Sarioglu H, Vogt-Weisenhorn DM, Wurst W, Gloeckner CJ, Matteoli M, Sala C, Ueffing M.** 2011. LRRK2 controls synaptic vesicle storage and mobilization within the recycling pool. J Neurosci **31:**2225–2237. http://dx.doi.org/10.1523/JNEUROSCI.3730-10.2011.
16. **Alegre-Abarrategui J, Christian H, Lufino MM, Mutihac R, Venda LL, Ansorge O, Wade-Martins R.** 2009. LRRK2 regulates autophagic activity and localizes to specific membrane microdomains in a novel human genomic reporter cellular model. Hum Mol Genet **18:**4022–4034. http://dx.doi.org/10.1093/hmg/ddp346.
17. **Manzoni C, Mamais A, Dihanich S, McGoldrick P, Devine MJ, Zerle J, Kara E, Taanman JW, Healy DG, Marti-Masso JF, Schapira AH, Plun-Favreau H, Tooze S, Hardy J, Bandopadhyay R, Lewis PA.** 2013. Pathogenic Parkinson's disease mutations across the functional domains of LRRK2 alter the autophagic/lysosomal response to starvation. Biochem Biophys Res Commun **441:**862–866. http://dx.doi.org/10.1016/j.bbrc.2013.10.159.
18. **Plowey ED, Cherra SJ, III, Liu YJ, Chu CT.** 2008. Role of autophagy in G2019S-LRRK2-associated neurite shortening in differentiated SH-SY5Y cells. J Neurochem **105:**1048–1056. http://dx.doi.org/10.1111/j.1471-4159.2008.05217.x.
19. **Ramonet D, Daher JP, Lin BM, Stafa K, Kim J, Banerjee R, Westerlund M, Pletnikova O, Glauser L, Yang L, Liu Y, Swing DA, Beal MF, Troncoso JC, McCaffery JM, Jenkins NA, Copeland NG, Galter D, Thomas B, Lee MK, Dawson TM, Dawson VL, Moore DJ.** 2011. Dopaminergic neuronal loss, reduced neurite complexity and autophagic abnormalities in transgenic mice expressing G2019S mutant LRRK2. PLoS One **6:**e18568. http://dx.doi.org/10.1371/journal.pone.0018568.
20. **Tong Y, Giaime E, Yamaguchi H, Ichimura T, Liu Y, Si H, Cai H, Bonventre JV, Shen J.** 2012. Loss of leucine-rich repeat kinase 2 causes age-dependent bi-phasic alterations of the autophagy pathway. Mol Neurodegener **7:**2. http://dx.doi.org/10.1186/1750-1326-7-2.
21. **Taylor JP, Hulihan MM, Kachergus JM, Melrose HL, Lincoln SJ, Hinkle KM, Stone JT, Ross OA, Hauser R, Aasly J, Gasser T, Payami H, Wszolek ZK, Farrer MJ.** 2007. Leucine-rich repeat kinase 1: a paralog of LRRK2 and a candidate gene for Parkinson's disease. Neurogenetics **8:**95–102. http://dx.doi.org/10.1007/s10048-006-0075-8.
22. **Gómez-Suaga P, Rivero-Rios P, Fdez E, Blanca Ramirez M, Ferrer I, Aiastui A, Lopez De Munain A, Hilfiker S.** 2014. LRRK2 delays degradative receptor trafficking by impeding late endosomal budding through decreasing Rab7 activity. Hum Mol Genet **23:**6779–6796. http://dx.doi.org/10.1093/hmg/ddu395.
23. **MacLeod DA, Rhinn H, Kuwahara T, Zolin A, Di Paolo G, McCabe BD, Marder KS, Honig LS, Clark LN, Small SA, Abeliovich A.** 2013. RAB7L1 interacts with LRRK2 to modify intraneuronal protein sorting and Parkinson's disease risk. Neuron **77:**425–439. http://dx.doi.org/10.1016/j.neuron.2012.11.033.
24. **Xu, J.** 2005. Preparation, culture, and immortalization of mouse embryonic fibroblasts. Curr Protoc Mol Biol **Chapter 28:**Unit 28.1.
25. **Smith WW, Pei Z, Jiang H, Dawson VL, Dawson TM, Ross CA.** 2006. Kinase activity of mutant LRRK2 mediates neuronal toxicity. Nat Neurosci **9:**1231–1233. http://dx.doi.org/10.1038/nn1776.
26. **Zach S, Felk S, Gillardon F.** 2010. Signal transduction protein array analysis links LRRK2 to Ste20 kinases and PKC zeta that modulate neuronal plasticity. PLoS One **5:**e13191. http://dx.doi.org/10.1371/journal.pone.0013191.
27. **Spinosa MR, Progida C, De Luca A, Colucci AM, Alifano P, Bucci C.** 2008. Functional characterization of Rab7 mutant proteins associated with Charcot-Marie-Tooth type 2B disease. J Neurosci **28:**1640–1648. http://dx.doi.org/10.1523/JNEUROSCI.3677-07.2008.
28. **Mortimore GE, Poso AR.** 1987. Intracellular protein catabolism and its control during nutrient deprivation and supply. Annu Rev Nutr **7:**539–564. http://dx.doi.org/10.1146/annurev.nu.07.070187.002543.
29. **Kuma A, Hatano M, Matsui M, Yamamoto A, Nakaya H, Yoshimori T, Ohsumi Y, Tokuhisa T, Mizushima N.** 2004. The role of autophagy during the early neonatal starvation period. Nature **432:**1032–1036. http://dx.doi.org/10.1038/nature03029.
30. **Kabeya Y, Mizushima N, Ueno T, Yamamoto A, Kirisako T, Noda T, Kominami E, Ohsumi Y, Yoshimori T.** 2000. LC3, a mammalian homologue of yeast Apg8p, is localized in autophagosome membranes after processing. EMBO J **19:**5720–5728. http://dx.doi.org/10.1093/emboj/19.21.5720.
31. **Bjørkøy G, Lamark T, Pankiv S, Overvatn A, Brech A, Johansen T.** 2009. Monitoring autophagic degradation of p62/SQSTM1. Methods Enzymol **452:**181–197. http://dx.doi.org/10.1016/S0076-6879(08)03612-4.
32. **Grotemeier A, Alers S, Pfisterer SG, Paasch F, Daubrawa M, Dieterle A, Viollet B, Wesselborg S, Proikas-Cezanne T, Stork B.** 2010. AMPK-independent induction of autophagy by cytosolic Ca^{2+} increase. Cell Signal **22:**914–925. http://dx.doi.org/10.1016/j.cellsig.2010.01.015.
33. **Ogata M, Hino S, Saito A, Morikawa K, Kondo S, Kanemoto S, Murakami T, Taniguchi M, Tanii I, Yoshinaga K, Shiosaka S, Hammarback JA, Urano F, Imaizumi K.** 2006. Autophagy is activated for cell survival after endoplasmic reticulum stress. Mol Cell Biol **26:**9220–9231. http://dx.doi.org/10.1128/MCB.01453-06.
34. **Sarkar S, Davies JE, Huang Z, Tunnacliffe A, Rubinsztein DC.** 2007. Trehalose, a novel mTOR-independent autophagy enhancer, accelerates the clearance of mutant huntingtin and alpha-synuclein. J Biol Chem **282:**5641–5652. http://dx.doi.org/10.1074/jbc.M609532200.
35. **Kimura S, Noda T, Yoshimori T.** 2007. Dissection of the autophagosome maturation process by a novel reporter protein, tandem fluorescent-tagged LC3. Autophagy **3:**452–460. http://dx.doi.org/10.4161/auto.4451.
36. **Diwu Z, Chen CS, Zhang C, Klaubert DH, Haugland RP.** 1999. A novel acidotropic pH indicator and its potential application in labeling acidic organelles of live cells. Chem Biol **6:**411–418. http://dx.doi.org/10.1016/S1074-5521(99)80059-3.
37. **Li J, Mahajan A, Tsai MD.** 2006. Ankyrin repeat: a unique motif mediating protein-protein interactions. Biochemistry **45:**15168–15178. http://dx.doi.org/10.1021/bi062188q.
38. **Kobe B, Kajava AV.** 2001. The leucine-rich repeat as a protein recognition motif. Curr Opin Struct Biol **11:**725–732. http://dx.doi.org/10.1016/S0959-440X(01)00266-4.
39. **Chaineau M, Danglot L, Galli T.** 2009. Multiple roles of the vesicular-SNARE TI-VAMP in post-Golgi and endosomal trafficking. FEBS Lett **583:**3817–3826. http://dx.doi.org/10.1016/j.febslet.2009.10.026.
40. **Luzio JP, Pryor PR, Bright NA.** 2007. Lysosomes: fusion and function. Nat Rev Mol Cell Biol **8:**622–632. http://dx.doi.org/10.1038/nrm2217.
41. **Ueyama T, Kusakabe T, Karasawa S, Kawasaki T, Shimizu A, Son J, Leto TL, Miyawaki A, Saito N.** 2008. Sequential binding of cytosolic Phox complex to phagosomes through regulated adaptor proteins: evaluation using the novel monomeric Kusabira-Green System and live imaging of phagocytosis. J Immunol **181:**629–640. http://dx.doi.org/10.4049/jimmunol.181.1.629.
42. **Gutierrez MG, Munafo DB, Beron W, Colombo MI.** 2004. Rab7 is required for the normal progression of the autophagic pathway in mammalian cells. J Cell Sci **117:**2687–2697. http://dx.doi.org/10.1242/jcs.01114.
43. **Jäger S, Bucci C, Tanida I, Ueno T, Kominami E, Saftig P, Eskelinen EL.** 2004. Role for Rab7 in maturation of late autophagic vacuoles. J Cell Sci **117:**4837–4848. http://dx.doi.org/10.1242/jcs.01370.
44. **Carroll B, Mohd-Naim N, Maximiano F, Frasa MA, McCormack J, Finelli M, Thoresen SB, Perdios L, Daigaku R, Francis RE, Futter C, Dikic I, Braga VM.** 2013. The TBC/RabGAP Armus coordinates Rac1 and

Rab7 functions during autophagy. Dev Cell **25:**15–28. http://dx.doi.org/10.1016/j.devcel.2013.03.005.
45. **Bos JL, Rehmann H, Wittinghofer A.** 2007. GEFs and GAPs: critical elements in the control of small G proteins. Cell **129:**865–877. http://dx.doi.org/10.1016/j.cell.2007.05.018.
46. **Sanz-Moreno V, Gadea G, Ahn J, Paterson H, Marra P, Pinner S, Sahai E, Marshall CJ.** 2008. Rac activation and inactivation control plasticity of tumor cell movement. Cell **135:**510–523. http://dx.doi.org/10.1016/j.cell.2008.09.043.
47. **Frasa MA, Maximiano FC, Smolarczyk K, Francis RE, Betson ME, Lozano E, Goldenring J, Seabra MC, Rak A, Ahmadian MR, Braga VM.** 2010. Armus is a Rac1 effector that inactivates Rab7 and regulates E-cadherin degradation. Curr Biol **20:**198–208. http://dx.doi.org/10.1016/j.cub.2009.12.053.
48. **Drugan JK, Rogers-Graham K, Gilmer T, Campbell S, Clark GJ.** 2000. The Ras/p120 GTPase-activating protein (GAP) interaction is regulated by the p120 GAP pleckstrin homology domain. J Biol Chem **275:**35021–35027. http://dx.doi.org/10.1074/jbc.M004386200.
49. **Stenmark H.** 2009. Rab GTPases as coordinators of vesicle traffic. Nat Rev Mol Cell Biol **10:**513–525. http://dx.doi.org/10.1038/nrm2728.
50. **Martinez-Arca S, Rudge R, Vacca M, Raposo G, Camonis J, Proux-Gillardeaux V, Daviet L, Formstecher E, Hamburger A, Filippini F, D'Esposito M, Galli T.** 2003. A dual mechanism controlling the localization and function of exocytic v-SNAREs. Proc Natl Acad Sci U S A **100:**9011–9016. http://dx.doi.org/10.1073/pnas.1431910100.
51. **Pryor PR, Jackson L, Gray SR, Edeling MA, Thompson A, Sanderson CM, Evans PR, Owen DJ, Luzio JP.** 2008. Molecular basis for the sorting of the SNARE VAMP7 into endocytic clathrin-coated vesicles by the Arf-GAP Hrb. Cell **134:**817–827. http://dx.doi.org/10.1016/j.cell.2008.07.023.
52. **Behrends C, Sowa ME, Gygi SP, Harper JW.** 2010. Network organization of the human autophagy system. Nature **466:**68–76. http://dx.doi.org/10.1038/nature09204.
53. **Popovic D, Akutsu M, Novak I, Harper JW, Behrends C, Dikic I.** 2012. Rab GTPase-activating proteins in autophagy: regulation of endocytic and autophagy pathways by direct binding to human ATG8 modifiers. Mol Cell Biol **32:**1733–1744. http://dx.doi.org/10.1128/MCB.06717-11.
54. **Beilina A, Rudenko IN, Kaganovich A, Civiero L, Chau H, Kalia SK, Kalia LV, Lobbestael E, Chia R, Ndukwe K, Ding J, Nalls MA, Olszewski M, Hauser DN, Kumaran R, Lozano AM, Baekelandt V, Greene LE, Taymans JM, Greggio E, Cookson MR.** 2014. Unbiased screen for interactors of leucine-rich repeat kinase 2 supports a common pathway for sporadic and familial Parkinson disease. Proc Natl Acad Sci U S A **111:**2626–2631. http://dx.doi.org/10.1073/pnas.1318306111.
55. **Nordmann M, Cabrera M, Perz A, Brocker C, Ostrowicz C, Engelbrecht-Vandre S, Ungermann C.** 2010. The Mon1-Ccz1 complex is the GEF of the late endosomal Rab7 homolog Ypt7. Curr Biol **20:**1654–1659. http://dx.doi.org/10.1016/j.cub.2010.08.002.
56. **Peralta ER, Martin BC, Edinger AL.** 2010. Differential effects of TBC1D15 and mammalian Vps39 on Rab7 activation state, lysosomal morphology, and growth factor dependence. J Biol Chem **285:**16814–16821. http://dx.doi.org/10.1074/jbc.M110.111633.
57. **Poteryaev D, Datta S, Ackema K, Zerial M, Spang A.** 2010. Identification of the switch in early-to-late endosome transition. Cell **141:**497–508. http://dx.doi.org/10.1016/j.cell.2010.03.011.
58. **Marín I.** 2006. The Parkinson disease gene LRRK2: evolutionary and structural insights. Mol Biol Evol **23:**2423–2433. http://dx.doi.org/10.1093/molbev/msl114.
59. **Dodson MW, Zhang T, Jiang C, Chen S, Guo M.** 2012. Roles of the Drosophila LRRK2 homolog in Rab7-dependent lysosomal positioning. Hum Mol Genet **21:**1350–1363. http://dx.doi.org/10.1093/hmg/ddr573.